Designing Soft Pyroelectric and Electrocaloric Materials Using Electrets

Faezeh Darbaniyan[*], Kaushik Dayal[†], Liping Liu[‡], Pradeep Sharma[§],

[*§]Department of Mechanical Engineering, University of Houston, Houston, TX 77204, USA

[†]Department of Civil and Environmental Engineering, Carnegie Mellon University

[†]Center for Nonlinear Analysis, Carnegie Mellon University

[†]Department of Materials Science and Engineering, Carnegie Mellon University

[‡]Department of Mathematics, Rutgers University, NJ 08854, USA

[‡]Department of Mechanical Aerospace Engineering, Rutgers University, NJ 08854, USA

[§]Department of Physics, University of Houston, Houston, TX 77204, USA.

April 28, 2019

Abstract

A temperature variation can electrically polarize a pyroelectric material. In its converse manifestation, the electrocaloric effect entails the change in temperature due to the application of an electric field. These phenomena have wide applications ranging from infrared detection sensors, solid-state refrigeration to energy harvesting. However, the pyroelectric-electrocaloric effect is typically observed in certain classes of hard, brittle crystalline materials that must satisfy a stringent set of lattice symmetry conditions. Some limited experiments have however demonstrated that embedding immobile charges and dipoles in soft foams (thus creating an electret state) may lead to a pyroelectric-like response as well as large deformations desired from soft matter. In this work, we develop a systematic theory for coupled electrical, thermal and mechanical response of soft electrets. Using simple illustrative examples, we derive closed-form explicit expressions for the pyroelectric and electrocaloric coefficients of electrets. While pyroelectricity in electrets has been noted before, our derived expressions provide a clear quantitative basis to interpret (and eventually design) this effect as well as insights into how the geometrically nonlinear deformation and Maxwell stress give rise to its emergence. We present conditions to obtain larger pyroelectric and electrocaloric response. In particular, the electrocaloric effect is predicted for the first time in such materials and we show that a proper design and a reasonable choice of materials can lead to a temperature reduction of as much as $1.5K$ under the application of electrical fields of $10MV/cm$.

[*]Email: faeze.darbaniyan@gmail.com
[†]Email: Kaushik.Dayal@cmu.edu
[‡]Email: liu.liping@rutgers.edu
[§]Email: psharma@uh.edu

1 Introduction

A class of hard, brittle ferroelectric ceramics possess the remarkable ability to convert temperature variations into electricity[1]. Examples of such pyroelectric materials include barium titanate, barium strontium titanate lead zirconate titanate among others. Thermodynamics dictates that pyroelectric materials also display the converse (so-called) *electrocaloric* effect whereby upon application of an electric field, a change in temperature in the material is observed. Thermal imaging, infrared detection sensors, energy harvesting, thermal actuators, and solid-state refrigeration are some of the possible applications of pyroelectric-electrocaloric materials [BTL+14, XMG+10, MXLM11, VYP08, WSJ76, BP89, WE14, Nal95].

A soft material with an ability to sustain large mechanical deformations *and* convert a temperature change into electricity makes for an intriguing combination. The motivation to develop soft multifunctional materials hardly needs to be emphasized—-numerous contexts such as soft robotics and stretchable electronics among others require the development of such materials [BBGG+14, CBDR10, HSSC13, LCM05, RSH10, YZS17, KGBA16]. The hard ferroelectric ceramics that exhibit pyroelectricity, in addition to being expensive, are unsuitable for applications that necessitate large-deformations. Some polymers such as polyvinylidene fluoride (PVDF) are also pyroelectric but the effect is quite weak in comparison to the hard ceramics (for the best case, one orders of magnitude less [Wha86, SOS+91]) and at a typical elastic modulus of a few GPa, materials like PVDF are not quite considered as *soft*.

The concept of electret materials may offer a possible recourse to create soft materials with an appreciable pyroelectric and electrocaloric response [NSBG+01]. Electret materials are simply dielectrics with embedded *immobile* or *trapped* charges and dipoles [VTSWdH99, Qiu10, JA18, MKR+08](Figure 1)[2]. While the basic notion of electrets can be tracked to the early part of the last century, these materials acquired engineering prominence by the work of groups led by Sessler, Gerhard-Multhaupt, Gross and Bauer [BGMS04, SS80, SH99, GM87, BSB08, WB05] who fabricated soft polymer foams containing large dipoles inserted on the void surfaces by the process of corona charging[3]. An often cited work [HS08], showed that a polypropylene electret foam exhibits an apparent piezoelectric coefficient of $1200pC/N$ which is nearly six times larger than the arguably most often used ferroelectric piezoelectric ceramic: lead zirconium titanate. While simple (and insightful) models have been proposed that explain piezoelectricity in such electret materials, recent theoretical modeling has clearly shown that the emergence of the piezoelectric-like response in such (otherwise non-piezoelectric materials) is due to the interaction of Maxwell

[1] We remark that the so-called thermoelectrics can also convert thermal energy into electricity however those are fundamentally different from pyroelectric materials. Thermoelectrics require a spatially varying temperature field, i.e. temperature gradients, while in a pyroelectric material, a uniform change in temperature is sufficient to yield an electrical response. There are other differences as well, however, a detailed discussion of thermoelectrics would be a digression for the purposes of this paper.

[2] The electret state is necessarily metastable. However, for many typical polymer foams which have been used to create electrets, the charges and dipoles can be stabilized at room temperature for years to decades.

[3] A discussion on the various approaches to *make* electrets is beyond the scope of the present work. The reader is referred to the following resources and references therein for further information.

stress (or electrostriction), deformation nonlinearity and the presence of the charges or dipoles [DLS14, ADLS15].

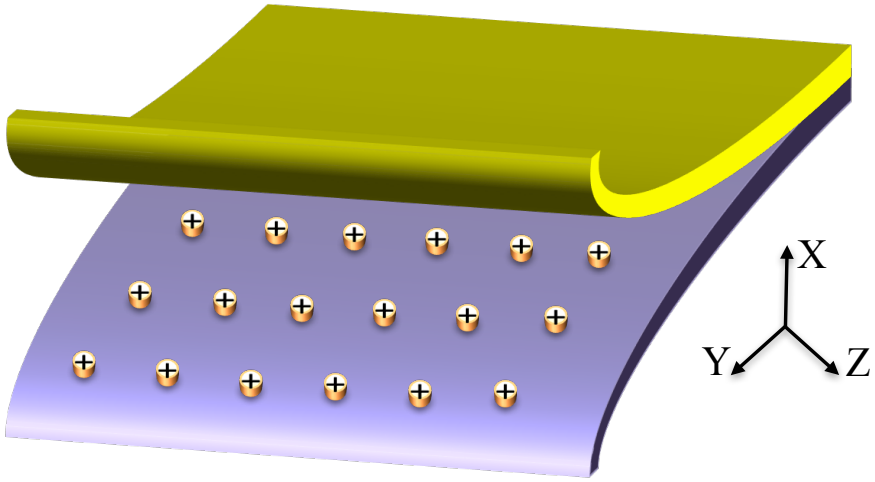

Figure 1 A schematic of a layered electret material consisting of two different films and an electric charge at the interface.

In the present work, we explore the possibility of using electrets to design a high pyroelectric and electrocaloric response (Figure 2). Past works have noted the emergence of a strong piezoelectric response but only a *weak* pyroelectric behavior has been observed [NSBG+01]. In fact, the work by Neugschwandtner, et al. [NSBG+01] showed the pyroelectric coefficient of electret foam to be several orders of magnitude *less* than pyroelectric ceramics and/or crystals. We remark that, to the best of our knowledge, there exists no experimental or theoretical work that has measured or estimated the electrocaloric response of electrets. To better understand the origin of apparent pyroelectricity and electrocaloric effect in electrets and to design such materials, there is a need for a theoretical framework which we proceed to establish in this paper. Using the developed theoretical framework, and simple illustrative examples, we derive analytical expressions that yield insights into obtaining higher pyroelectric and electrocaloric response from soft electret materials.

In Section 2, we present the theoretical framework to couple large (nonlinear) mechanical deformation, pre-existing charges and dipoles, thermal transport and electrical behavior. Other works exist that have presented coupled thermo-electro-elastic theories e.g. [AUV06, VBPCB13, CEG78, CG77, SVS14, MHS16, MPS17]. Rather than modifying the existing approaches to address electrets, we prefer an approach that uses polarization as an independent state-variable and a treatment inspired by Xiao and Bhattacharya's work [XB08] on treating the non-equilibrium mechanics of semiconductor ferroelectrics[4]. In Sections 2.5 and 2.8 we solve the derived equations for a simple two-layer and porous foam electret material design to illustrate the emergent pyroelectric and electrocaloric respectively.

[4] A recent exposition which compares various flavors of electro-elastic theories can be found in the two papers by Liu [Liu13, Liu14]

2 Theoretical Formulation

The great success of continuum mechanics lies in a clear separation of equations of different origins, namely, the universal physical laws, e.g. the conservation laws, Maxwell equations and thermodynamic laws, and the material specific kinematics and constitutive relations. Following this paradigm, in this section we present a continuum framework that will allow us to address the couplings between elasticity, thermal transport, electrostatics, and pre-existing charges. We have tried to keep our formulation as general as possible so that it is applicable beyond the simple illustrative examples studied in the present work.

2.1 Kinematics

We first need to specify the thermodynamic system including the state variables and the boundary and loading conditions. This is always necessary to apply the thermodynamic laws without ambiguity. To model materials with couplings between elasticity, electrostatics and thermal transport, we consider a deformable body $\Omega_R \subset \mathbb{R}^3$, as shown in Figure 3. The position of a material point in the reference (Ω_R) and spatial (Ω_t) configurations is specified by Lagrangian coordinates $\mathbf{X} \in \Omega_R$ and Eulerian coordinates $\mathbf{x} \in \Omega_t$, respectively. As usual, denote by

$$\mathbf{F} = \nabla \mathbf{x}, \quad \mathbf{C} = \boldsymbol{F}^T \boldsymbol{F}, \quad J = \det \boldsymbol{F} \tag{2.1}$$

the deformation gradient, the right Cauchy-Green tensor, and the Jacobian of the deformation gradient, respectively.

Notation and terminology. For clarity, we refer to "the system" as the material body Ω_R and the associated external boundary and loading conditions. It is the system (not the body) that can be treated as thermodynamically closed and isolated. For brevity, wherever possible, we employ direct notation. Vectors are denoted by bold symbols such as $\boldsymbol{e}, \boldsymbol{u}$, etc. The tensor product between two vectors $\boldsymbol{a}, \boldsymbol{b} \in \mathbb{R}^3$ is defined as $(\boldsymbol{a} \otimes \boldsymbol{b})_{ij} = (\boldsymbol{a})_i (\boldsymbol{b})_j$ whereas the inner (or dot) product is defined as $\langle \boldsymbol{a}, \boldsymbol{b} \rangle \equiv \boldsymbol{a} \cdot \boldsymbol{b} := (\boldsymbol{a})_i (\boldsymbol{b})_i$, and the inner (or dot) product between matrices $\boldsymbol{A}$ and $\boldsymbol{B}$ of the same size is defined as $\boldsymbol{A} \cdot \boldsymbol{B} := \mathrm{Tr}(\boldsymbol{A}^T \boldsymbol{B}) = (\boldsymbol{A})_{ij} (\boldsymbol{B})_{ij}$. Operators ∇ and div are taken with respect to the Lagrangian coordinates $\boldsymbol{X}$ whereas $\nabla_{\boldsymbol{x}}$ and $\mathrm{div}_{\boldsymbol{x}}$ are taken with respect to the Eulerian coordinates $\boldsymbol{x}$. From the viewpoint of matrices, the i^{th} row vector of the gradient of a vector field, e.g., $\nabla \boldsymbol{u} = \partial \boldsymbol{u}_i / \partial \boldsymbol{X}_j = \boldsymbol{u}_{i,j}$, whereas the "div" operates on the row vectors of a matrix field. Therefore, $\mathrm{div} \nabla \boldsymbol{u} = \Delta \boldsymbol{u} = \partial^2 \boldsymbol{u}_i / \partial \boldsymbol{X}_j^2$ and $\mathrm{div}[(\nabla \boldsymbol{u})^T] = \nabla(\mathrm{div} \boldsymbol{u}) = \partial^2 \boldsymbol{u}_j / \partial \boldsymbol{X}_i \partial \boldsymbol{X}_j$.

Our starting point is the claim that the thermodynamic state of the body is described by the deformation $\boldsymbol{x}(\cdot, t) : \Omega_R \to \Omega_t$, nominal polarization $\boldsymbol{P}(\cdot, t) : \Omega_R \to \mathbb{R}^3$ (representing the dipole density per unit volume in the reference configuration), and temperature $T(\cdot, t) : \Omega_R \to \mathbb{R}$, and the postulation (P1) that there exists a free energy density $\Psi : \mathbb{R}^{3\times 3} \times \mathbb{R}^3 \times \mathbb{R}^+ \to \mathbb{R}$ such that the *total* free energy of the body is given by (including the contribution from the electric field but not the boundary devices)

$$A[\boldsymbol{x}, \boldsymbol{P}, T] = \int_{\Omega_R} \Psi(\nabla \boldsymbol{x}, \boldsymbol{P}, T) + \mathcal{E}[\boldsymbol{x}, \boldsymbol{P}], \tag{2.2}$$

where the first term prescribes the equilibrium response of the material, and the second term arises from the field energy associated with the electric field which will be specified momentarily. Noticing that the second term is independent of temperature T, we identify

$$S(\boldsymbol{F}, \boldsymbol{P}, T) := -\frac{\partial}{\partial T}\Psi(\boldsymbol{F}, \boldsymbol{P}, T) \tag{2.3}$$

as the local entropy density (per unit volume in the reference configuration). From thermodynamics we identify the internal energy density in the absence of electric field as

$$\Phi(\boldsymbol{F}, \boldsymbol{P}, T) := \Psi(\boldsymbol{F}, \boldsymbol{P}, T) + TS(\boldsymbol{F}, \boldsymbol{P}, T), \tag{2.4}$$

and the total internal energy of the body as

$$U[\boldsymbol{x}, \boldsymbol{P}, T] = \int_{\Omega_R} \Phi(\nabla \boldsymbol{x}, \boldsymbol{P}, T) + \mathcal{E}[\boldsymbol{x}, \boldsymbol{P}]. \tag{2.5}$$

We remark that the functions Ψ, S, Φ in Eqs.(2.2)-(2.4) do not explicitly depend on $(\boldsymbol{X}, t)$, implying that the body is homogeneous in space and time.

To apply the first and second laws of thermodynamics to the system, we need to specify the mechanical, electrostatic, and thermal interactions between the body and the external devices including the precise boundary conditions on the state variables (or their conjugates or related quantities) and external mechanical, electrostatic and thermal loading conditions. By the Maxwell equations, we introduce the electric potential $\xi : \Omega_R \to \mathbb{R}$ such that $-\nabla_{\boldsymbol{x}}\xi = -\mathbf{F}^{-T}\nabla\xi$ is the spatial electric field, $\boldsymbol{e}$, in the current configuration.

While more general boundary conditions may be considered, for ease of presentation and notation we focus only on the Dirichlet-type boundary conditions:

$$\begin{cases} \mathbf{x}(\boldsymbol{X}, t) = \mathbf{X} + \boldsymbol{u}_b(\boldsymbol{X}, t) & \text{on } \partial\Omega_R, \\ \xi(\boldsymbol{X}, t) = \xi_b(\boldsymbol{X}, t) & \text{on } \partial\Omega_R, \\ T(\boldsymbol{X}, t) = T_b(\boldsymbol{X}, t) & \text{on } \partial\Omega_R, \end{cases} \tag{2.6}$$

where $\boldsymbol{u}_b(\text{resp. } \xi_b,\ T_b) : \partial\Omega_R \to \mathbb{R}^3(\text{resp. } \mathbb{R},\ \mathbb{R})$ is the prescribed boundary displacement (resp. electric potential, temperature). In addition, we assume that there are body force, charge and heat supply (per unit volume in the reference configuration):

$$\begin{cases} \text{applied body force} : \mathbf{b}_e(\boldsymbol{X}, t) & \text{in } \Omega_R, \\ \text{external charge density} : \rho_e(\boldsymbol{X}) & \text{in } \Omega_R, \\ \text{rate of heat supply} : r_e(\boldsymbol{X}, t) & \text{in } \Omega_R. \end{cases} \tag{2.7}$$

Here the external charges are assumed to be immobile[5] Notably, by definition, in electret materials, charges are not mobile on the time-scales of engineering interest. The charges are considered to be

[5]For an interesting exception to the case where charges are deemed immobile, the reader may consult the work on so-called “active" charges [LLP17].

attached to material points and hence independent of t when viewed from the reference configuration. If not, we would have to treat charge density as a state variable and specify the constitutive law to determine how charges move.

Now we define the electric field energy $\mathcal{E}$ in Eq.(2.2). Let ε_0 be the vacuum permitivity. The Maxwell equations imply that

$$\mathrm{div}_{\boldsymbol{x}}(-\epsilon_0 \nabla_{\boldsymbol{x}} \xi + \boldsymbol{P}/J) = \rho_e/J \qquad \text{in } \ \Omega_t, \tag{2.8}$$

in which $\boldsymbol{d} := -\epsilon_0 \nabla_{\boldsymbol{x}} \xi + \boldsymbol{P}/J$ is the electric displacement in current configuration. Eq.(2.8) in the reference configuration can be rewritten as

$$\mathrm{div}\boldsymbol{D} = \rho_e, \quad \boldsymbol{D} := -\varepsilon_0 J \mathbf{C}^{-1} \nabla \xi + \mathbf{F}^{-1}\mathbf{P} \qquad \text{in } \ \Omega_R, \tag{2.9}$$

The above equation, together with the boundary condition e.g. Eq.$(2.6)_2$, determine the local electric field, and henceforth the energy contributed by the electric field:

$$\mathcal{E}[\boldsymbol{x}, \boldsymbol{P}] = \int_{\Omega_t} \frac{\varepsilon_0}{2} |\nabla_{\boldsymbol{x}} \xi|^2 = \int_{\Omega_R} \frac{\varepsilon_0}{2} J |\mathbf{F}^{-T} \nabla \xi|^2. \tag{2.10}$$

It will be of interest to calculate the time derivative of electric field energy $\mathcal{E}$, which is rather tedious and the details are recorded in Appendix A. We simply quote the final result here:

$$\frac{d}{dt}\mathcal{E} = \int_{\Omega_R} (\nabla \dot{\mathbf{x}} \cdot \boldsymbol{\Sigma}_{\mathrm{MW}} + \nabla \xi \cdot \mathbf{F}^{-1}\dot{\mathbf{P}}) - \int_{\partial \Omega_R} \xi_b \mathbf{n} \cdot \dot{\boldsymbol{D}}. \tag{2.11}$$

Here and subsequently, d/dt denotes the material time derivative and is sometimes written as $\dot{(\,)}$ for brevity. Also, the physical interpretation of $\dot{\boldsymbol{D}} \cdot \boldsymbol{n}$ is the electric current density flowing out the reference interface $\partial \Omega_R$, and $\boldsymbol{\Sigma}_{\mathrm{MW}}$ is the Maxwell stress:

$$\begin{aligned} \boldsymbol{\Sigma}_{\mathrm{MW}}[\nabla \boldsymbol{x}, \boldsymbol{P}] =& (\mathbf{F}^{-T} \nabla \xi) \otimes (\varepsilon_0 J \mathbf{C}^{-1} \nabla \xi - \mathbf{F}^{-1}\mathbf{P}) \\ & - \frac{\varepsilon_0}{2} J |\mathbf{F}^{-T} \nabla \xi|^2 \mathbf{F}^{-T}. \end{aligned} \tag{2.12}$$

The devices used to maintain the boundary conditions, Eq.(2.6), is used to describe the interaction with the body. The interaction "forces", albeit unknown, are denoted as follows:

$$\begin{cases} \text{external surface traction : } \mathbf{t}_e(\boldsymbol{X}, t) & \text{on } \partial_+ \Omega_R, \\ \text{heat flux into the body: } h_e(\boldsymbol{X}, t) & \text{on } \partial_+ \Omega_R, \\ \text{surface charge density: } \sigma_e(\boldsymbol{X}, t) & \text{on } \partial_+ \Omega_R, \end{cases} \tag{2.13}$$

where $\partial_+ \Omega_R$ represents the exterior boundary values (in the external devices).

To address the thermal conduction inside the body Ω_R, we invoke the concept of thermal flux $\boldsymbol{q}(\cdot, t) : \Omega_R \to \mathbb{R}^3$ such that for any part of the body $P \subset \Omega_R$,

$$-\int_{\partial P} \boldsymbol{q} \cdot \boldsymbol{n} + \int_P r_e$$

is the rate of heat into the subbody P. Across the interface $\partial\Omega_R$, the conservation of energy and Gauss's law of electrostatics imply that

$$h_e = -\boldsymbol{q}\cdot\boldsymbol{n}, \quad \sigma_e = -\boldsymbol{D}\cdot\boldsymbol{n} \qquad \text{on } \partial\Omega_R. \tag{2.14}$$

We can now identify the rate of work done to the body (by the external devices) as:

$$P_{\text{ext}} = \int_{\partial\Omega_R} \dot{\boldsymbol{u}}_b\cdot\mathbf{t}_e + \int_{\Omega_R}\dot{\mathbf{x}}\cdot\mathbf{b}_e + \int_{\partial\Omega_R}\xi_b\dot{\sigma}_e, \tag{2.15}$$

and the rate of heat transferred into the body is given by:

$$\dot{Q} = \int_{\partial\Omega_R} h_e + \int_{\Omega_R} r_e. \tag{2.16}$$

We denote the rate of energy dissipation per unit (reference) volume by

$$\Gamma := T\dot{S} - r_e + T\text{div}(\frac{\mathbf{q}}{T}) \qquad \text{in } \Omega_R. \tag{2.17}$$

Integrating the above equation over Ω_R, by Eq.(2.14), Eq.(2.16), and the divergence theorem, we find that the heat supplied to the body can be rewritten as

$$\dot{Q} = -\int_{\Omega_R}(\Gamma - T\dot{S} + \frac{1}{T}\mathbf{q}\cdot\nabla T). \tag{2.18}$$

2.2 The first and second laws

The thermodynamic laws place strong restrictions on the constitutive laws of the material and the actual thermodynamic process of the system. Neglecting the kinetic energy of the body, by the first law of thermodynamics we have $\dot{U} = P_{\text{ext}} + \dot{Q}$, and hence, by Eqs.(2.4), (2.5) and (2.18),

$$\int_{\Omega_R}(\dot{\Psi} + S\dot{T} + \Gamma + \frac{1}{T}\boldsymbol{q}\cdot\nabla T) + \dot{\mathcal{E}} = P_{\text{ext}}, \tag{2.19}$$

Let

$$\boldsymbol{\Sigma}[\nabla\boldsymbol{x}, \boldsymbol{P}] = \frac{\partial\Psi}{\partial\boldsymbol{F}}(\nabla\boldsymbol{x}, \boldsymbol{P}, T) + \boldsymbol{\Sigma}_{\text{MW}}[\nabla\boldsymbol{x}, \boldsymbol{P}] \tag{2.20}$$

be the total Piola-Kirchhoff stress field in the body. Using Eqs.(2.11) and (2.15) we rewrite Eq.(2.19) as

$$\hat{L} = 0, \tag{2.21}$$

where

$$\begin{aligned} -\hat{L} := \int_{\Omega_R}\Big[&\boldsymbol{\Sigma}\cdot\nabla\dot{\boldsymbol{x}} - \boldsymbol{b}_e\cdot\dot{\boldsymbol{x}} + (\frac{\partial\Psi}{\partial\mathbf{P}} + \mathbf{F}^{-T}\nabla\xi)\cdot\dot{\mathbf{P}} \\ &+ (\Gamma + \frac{1}{T}\mathbf{q}\cdot\nabla T)\Big] - \int_{\partial\Omega_R}\mathbf{t}_e\cdot\dot{\mathbf{u}}_b. \end{aligned} \tag{2.22}$$

The quantity $\hat{L}$ may be identified as the first variation of the classic Lagrangian (or the potential energy since the kinetic energy is neglected) of the system upon neglecting thermal conduction and energy dissipation ($\boldsymbol{q} \equiv 0$, $\Gamma \equiv 0$).

Next, the second law of thermodynamics implies the Clausius-Duhem inequality (Gurtin, et al, pg 187) [GFA10]:

$$\frac{d}{dt}\int_P S \geq -\int_{\partial P} \frac{\mathbf{q}\cdot\mathbf{n}}{T} + \int_P \frac{r_e}{T}, \tag{2.23}$$

where $P \subset \Omega_R$ is any material volume element in the reference configuration. Applying the divergence theorem to the surface integral on the right of Eq.(2.23), we obtain the local differential form:

$$\Gamma = T\dot{S} - r_e + T\mathrm{div}(\frac{\boldsymbol{q}}{T}) \geq 0 \qquad \text{in } \ \Omega_R. \tag{2.24}$$

The above inequality justifies the terminology for Γ as the " rate of energy dissipation" (per unit volume).

To achieve a local differential form associated with the global energy balance, Eq.(2.19), we make additional constitutive postulations concerning the non-equilibrium processes (P2). The rate of energy dissipation density Γ and heat flux $\boldsymbol{q}$ depends locally on $(\nabla T, \boldsymbol{F}, \boldsymbol{P}, T)$ but not the rates $(\dot{\boldsymbol{F}}, \dot{\boldsymbol{P}}, \dot{T})$:

$$\Gamma = \Gamma(\nabla T, \boldsymbol{F}, \boldsymbol{P}, T), \quad \boldsymbol{q} = \boldsymbol{q}(\nabla T, \boldsymbol{F}, \boldsymbol{P}, T). \tag{2.25}$$

We remark that the two functions $\Gamma, \boldsymbol{q}$ depend on each other. In Appendix B, for the sake of completeness, we have considered a more general form of rate-dependent dissipation function Γ to potentially allow for other dissipative effects such as viscosity.
Now, by Eq.(2.25) we see that the quantity $\hat{L}$ in Eq.(2.22) is uniquely defined at *any instance e.g.* $t = t_0$ if the state variables $(\boldsymbol{x}(\boldsymbol{X}, t_0), \boldsymbol{P}(\boldsymbol{X}, t_0), T(\boldsymbol{X}, t_0))$ and the rate of changes $(\dot{\boldsymbol{x}}(\boldsymbol{X}, t_0), \dot{\boldsymbol{P}}(\boldsymbol{X}, t_0))$ are specified. Of course, $\hat{L}$ depends on the external conditions as well — $\boldsymbol{t}_e, \boldsymbol{b}_e, \rho_e, \xi_b$. We may now apply the traditional arguments on the lines of the Coleman-Noll procedure without explicitly identifying the dissipative forces, and claim that (#) *at any instance e.g.* $t = t_0$ *and for the instantaneous state* $(\boldsymbol{x}(\boldsymbol{X}, t_0), \boldsymbol{P}(\boldsymbol{X}, t_0), T(\boldsymbol{X}, t_0))$*, the first law Eq.*(2.19) *holds for* any kinematically *admissible rates of change* $(\dot{\boldsymbol{x}}(\cdot, t_0), \dot{\boldsymbol{P}}(\cdot, t_0), T(\cdot, t_0)) \in \mathcal{U}$ *and any boundary and loading conditions.* Here, the kinematically admissible space for the rates of change is defined as: (The integrability and differentiability conditions are omitted here for brevity)

$$\mathcal{U} := \Big\{(\boldsymbol{v}, \boldsymbol{p}, \theta) : \Omega_R \to \mathbb{R}^3 \times \mathbb{R}^3 \times \mathbb{R} \mid \boldsymbol{v} = \dot{\boldsymbol{u}}_b, \ \theta = \dot{T}_b \text{ on } \ \partial\Omega_R\Big\}.$$

Immediately, by Eq.(2.22) and the divergence theorem we find that

$$\begin{aligned}\int_{\Omega_R} \Big[&- (\mathrm{div}\boldsymbol{\Sigma} + \boldsymbol{b}_e)\cdot\dot{\boldsymbol{x}} + (\frac{\partial\Psi}{\partial\mathbf{P}} + \mathbf{F}^{-T}\nabla\xi)\cdot\dot{\mathbf{P}} \\ &+ (\Gamma + \frac{1}{T}\mathbf{q}\cdot\nabla T)\Big] + \int_{\partial\Omega_R} (\boldsymbol{\Sigma}\boldsymbol{n} - \mathbf{t}_e)\cdot\dot{\mathbf{u}}_b = 0,\end{aligned} \tag{2.26}$$

and henceforth, the familiar local point-wise equations:

$$\begin{cases} \mathrm{div}\boldsymbol{\Sigma} = -\boldsymbol{b}_e & \text{in } \Omega_R, \\ \dfrac{\partial \Psi}{\partial \mathbf{P}} + \mathbf{F}^{-T}\nabla\xi = 0 & \text{in } \Omega_R, \\ \boldsymbol{\Sigma}\boldsymbol{n} = \boldsymbol{t}_e & \text{on } \partial\Omega_R, \end{cases} \tag{2.27}$$

and the integral equation:

$$\int_{\Omega_R} [\Gamma(\nabla T, \boldsymbol{F}, \boldsymbol{P}, T) + \frac{1}{T}\mathbf{q}(\nabla T, \boldsymbol{F}, \boldsymbol{P}, T) \cdot \nabla T] = 0. \tag{2.28}$$

By adjusting external conditions, the fields $(\nabla T, \boldsymbol{F}, \boldsymbol{P}, T)$ are presumably arbitrary on Ω_R, and hence an obvious constitutive assumption to guarantee Eq.(2.28) is to set that for any $(\boldsymbol{g}, \boldsymbol{F}, \boldsymbol{P}, T) \in \mathbb{R}^3 \times \mathbb{R}^{3\times 3} \times \mathbb{R}^3 \times \mathbb{R}^+$,

$$\Gamma(\boldsymbol{g}, \boldsymbol{F}, \boldsymbol{P}, T) = -\frac{1}{T}\boldsymbol{g} \cdot \mathbf{q}(\boldsymbol{g}, \boldsymbol{F}, \boldsymbol{P}, T). \tag{2.29}$$

By Eq.(2.17), the above constitutive assumption implies that

$$T\dot{S} - r_e + \mathrm{div}\boldsymbol{q} = \Gamma + \frac{1}{T}\mathbf{q} \cdot \nabla T = 0 \qquad \text{in } \Omega_R. \tag{2.30}$$

In conclusion, upon explicitly specifying the free energy function $\Psi = \Psi(\boldsymbol{F}, \boldsymbol{P}, T)$ and the energy dissipation function $\Gamma = \Gamma(\boldsymbol{g}, \boldsymbol{F}, \boldsymbol{P}, T)$, by Eqs.(2.3), (2.9), (2.27), and (2.30) we have the following partial differential system for $(\boldsymbol{x}, \xi, T)$:

$$\begin{cases} \mathrm{div}[\dfrac{\partial}{\partial \boldsymbol{F}}\Psi(\nabla\boldsymbol{x}, \boldsymbol{P}, T) + \boldsymbol{\Sigma}_{\mathrm{MW}}] = -\boldsymbol{b}_e & \text{in } \Omega_R, \\ \mathrm{div}[-\varepsilon_0 J\mathbf{C}^{-1}\nabla\xi + \mathbf{F}^{-1}\mathbf{P}] = \rho_e & \text{in } \Omega_R, \\ -T\dfrac{d}{dt}\dfrac{\partial}{\partial T}\Psi(\nabla\boldsymbol{x}, \boldsymbol{P}, T) - r_e + \mathrm{div}\boldsymbol{q} = 0 & \text{in } \Omega_R, \end{cases} \tag{2.31}$$

where $\boldsymbol{P}$, by inverting Eq.$(2.27)_2$, is regarded as a function of $(\boldsymbol{x}, \xi, T)$ and $(\nabla\boldsymbol{x}, \nabla\xi, \nabla T)$. Supplemented with the boundary conditions, Eq.(2.6), the differential system Eq.(2.31) may be solved to predict the equilibrium responses or the actual non-equilibrium processes of the system. Moreover, taking into account Eq.(2.14) and Eq.$(2.27)_3$ we can consider general mixed boundary conditions, e.g., $h_e, \sigma_e, \boldsymbol{t}_e$ are specified on part of $\partial\Omega_R$ whereas $\boldsymbol{u}_b, \xi_b, T_b$ are specified on the rest of $\partial\Omega_R$.

Finally, we remark that the above procedure to achieve the relations between the free energy function and stress i.e., Eq.(2.20) and dissipation function and heat flux i.e., Eq.(2.28) and the final differential equations Eq.(2.31) is not unique. Alternative approaches exist and to some extent, the approach is a matter of taste. From an axiomatic viewpoint we have assumed less primitive concepts (entropy S and stress $\boldsymbol{\Sigma}$ are now derived concepts), but a priori made stronger assumption that $\Psi, \Gamma, \boldsymbol{q}$ depend on $(\boldsymbol{X}, t)$ via the state variables $(\boldsymbol{x}, \boldsymbol{P}, T)$ (instead of just a function of $(\boldsymbol{X}, t)$ as in the typical Coleman-Noll procedure). The functional dependence of $\Psi, \Gamma, \boldsymbol{q}$ on the state variables has to be assumed anyway when it comes to specifying the constitutive laws. Therefore, we believe that our procedure is more convenient (at least to us) for formulating continuum theories of materials in dissipative processes where the precise concept of stress or dissipation mechanisms are elusive.

2.3 Constitutive relations and associated boundary value problems

In this section we make explicit constitutive choices by specifying the free energy function $\Psi = \Psi(\boldsymbol{F}, \boldsymbol{P}, T)$ and the rate of energy dissipation function $\Gamma = \Gamma(\boldsymbol{g}, \boldsymbol{F}, \boldsymbol{P}, T)$. We first consider restrictions on these functions as implied by the frame indifference, material symmetry, and judicial choice of reference configuration.

Let $SO(3)$ be the group including all rigid rotations and $\mathcal{G} \subset SO(3)$ be the subgroup associated with material symmetry. From the principle of frame indifference and material symmetry, we have that for any $\boldsymbol{R} \in SO(3)$,

$$\Psi(\boldsymbol{RF}, \boldsymbol{RP}, T) = \Psi(\boldsymbol{F}, \boldsymbol{P}, T), \quad \Gamma(\boldsymbol{g}, \boldsymbol{RF}, \boldsymbol{RP}, T) = \Gamma(\boldsymbol{g}, \boldsymbol{F}, \boldsymbol{P}, T), \tag{2.32}$$

and for any $\boldsymbol{Q} \in \mathcal{G}$,

$$\Psi(\boldsymbol{FQ}, \boldsymbol{P}, T) = \Psi(\boldsymbol{F}, \boldsymbol{P}, T), \quad \Gamma(\boldsymbol{Qg}, \boldsymbol{FQ}, \boldsymbol{P}, T) = \Gamma(\boldsymbol{g}, \boldsymbol{F}, \boldsymbol{P}, T). \tag{2.33}$$

By the second law, Eq.(2.24), we require that for any $(\boldsymbol{F}, \boldsymbol{P}, T) \in \mathbb{R}^{3\times3} \times \mathbb{R}^3 \times \mathbb{R}^+$,

$$\Gamma(\boldsymbol{g}, \boldsymbol{F}, \boldsymbol{P}, T) \geq 0 \; \forall \, \boldsymbol{g} \in \mathbb{R}^3 \qquad \text{and} \qquad \Gamma(0, \boldsymbol{F}, \boldsymbol{P}, T) = 0, \tag{2.34}$$

where the latter follows from the observation that the energy dissipation inside the body should vanish if the body is uniformly deformed and maintained at a constant polarization and temperature. Choosing the reference configuration as the natural configuration (i.e., the equilibrium configuration with $(\boldsymbol{P}, T) = (0, T_0)$ in the absence of external loadings: $(\boldsymbol{t}_e, \boldsymbol{b}_e, \rho_e, \sigma_e, h_e, r_e) \equiv 0$), we have

$$\Psi(\boldsymbol{F}, \boldsymbol{P}, T_0) \geq \Psi(\boldsymbol{I}, 0, T_0) \qquad \forall \, (\boldsymbol{F}, \boldsymbol{P}) \in \mathcal{N}(\boldsymbol{I}, 0), \tag{2.35}$$

where $\boldsymbol{I}$ is the identity matrix in $\mathbb{R}^{3\times3}$ and $\mathcal{N}(\boldsymbol{I}, 0)$ represents a neighborhood of $(\boldsymbol{I}, 0)$ in $\mathbb{R}^{3\times3}\times\mathbb{R}^3$.

The constitutive models, so far, are general (though more general dissipation function is discussed in the Appendix B), and may be used to tackle broad non-equilibrium processes involving large-deformation, thermal transport and electrostatics. In what follows, to simplify the generation of illustrative results, we assume that (i) the material is isotropic i.e. $\mathcal{G} = SO(3)$, (ii) the material is electrostatically an ideal dielectric material with permittivity ϵ independent of temperature and deformation, and since we are interested in soft materials, most of which are nearly incompressible, we assume that (iii) at constant temperature we have an incompressible neo-Hookean material. Notwithstanding the incompressibility assumption, thermoelasticity requires us to account for the volume change caused by thermal expansion. As outlined in Volokh [Vol16], the assumption of thermoelastic incompressibility may be incorporated in the following form using a Lagrange multiplier:

$$J = f(T), \qquad f(T_0) = 1 \tag{2.36}$$

We find that the following free energy density satisfies the assumption (i), (ii) and (iii):

$$\Psi(\boldsymbol{F}, \mathbf{P}, T) = \Psi(\boldsymbol{I}, 0, T) + \frac{\mu}{2}(I_1 - 3) - \Pi|J - f(T)| + \frac{a}{2J}|\mathbf{P}|^2, \tag{2.37}$$

where μ is the shear modulus of the neo-Hookean material, $|\cdot|$ denotes the absolute value, a is related to the dielectric constant of the material, and I_1 is the first invariant of the right Cauchy-Green deformation tensor: $I_1 = tr(\mathbf{C})$. A simple form of $\Psi(\boldsymbol{I}, 0, T)$ and $f(T)$ may be chosen as

$$\Psi(\boldsymbol{I}, 0, T) = \Psi_0 - CT \log T/T_0, \qquad f(T) = 1 + 3\alpha(T - T_0). \tag{2.38}$$

where Ψ_0 is a constant and can be identified as the free energy density at $(\boldsymbol{F}, \boldsymbol{P}, T) = (\boldsymbol{I}, 0, T_0)$, C is the heat capacity (per unit volume) and α is the linear thermal expansion coefficient of the material.

Concerning the dissipative processes, for simplicity we assume the dissipation function has the following quadratic form:

$$\Gamma(\boldsymbol{g}, \boldsymbol{F}, \boldsymbol{P}, T) = \frac{k}{T}|\boldsymbol{g}|^2, \tag{2.39}$$

or equivalently, by Eqs.(2.29) and (2.34), the linear Fourier's law:

$$\boldsymbol{q} = -k\nabla T, \tag{2.40}$$

For brevity, we denote by

$$\boldsymbol{u}(\boldsymbol{X}) = \boldsymbol{x}(\boldsymbol{X}) - \boldsymbol{X}, \quad \varepsilon = \epsilon_0 + 1/a, \quad \triangle T = T - T_0 \tag{2.41}$$

the displacement, electric permittivity of the material and temperature change from the reference temperature T_0.

2.4 Summary of governing equations

Recalling the identities:

$$\boldsymbol{F} = \nabla \boldsymbol{u} + \boldsymbol{I}, \qquad \frac{\partial}{\partial \boldsymbol{F}} J = J\boldsymbol{F}^{-T}.$$

and using the constitutive relations: Eqs.(2.37), (2.38), and (2.40), the governing equations, Eq.(2.31), for $(\boldsymbol{u}, \xi, T)$ can be obtained as:

$$\begin{cases} \operatorname{div}[\mu\boldsymbol{F} - \Pi J\boldsymbol{F}^{-T} - \dfrac{\varepsilon}{2}J|\mathbf{F}^{-T}\nabla\xi|^2\mathbf{F}^{-T} \\ \quad + \varepsilon J(\mathbf{F}^{-T}\nabla\xi) \otimes (\mathbf{C}^{-1}\nabla\xi)] = -\boldsymbol{b}_e & \text{in } \Omega_R, \\ \operatorname{div}(-\varepsilon J\mathbf{C}^{-1}\nabla\xi) = \rho_e & \text{in } \Omega_R, \\ C\dot{T} + 3\alpha T\dot{I} = r_e + \operatorname{div}(k\nabla T) & \text{in } \Omega_R, \end{cases} \tag{2.42}$$

We ignore stray electric fields that may, for instance, leak out of the non-electroded sides of the film (since in what follows, we have assumed that the thickness of the film is comparably small), but a possible extension to account for that is briefly described in Appendix C.

2.5 Emergent Pyroelectricity

To illustrate the basic ideas, obtain analytical solutions and insights into emergent pyroelectricity in electrets, we consider a heterogeneous system of two thin films with embedded charges at the interface (Figure 4). To investigate pyroelectricity, we assume that the system is initially maintained at zero voltage difference (i.e., short circuit) with a fixed boundary temperature (i.e., $T_b = T_0$) and traction free. To capture the essential effects that are of importance to present application, it is reasonable to assume piecewise uniform strain in each layer. By Eq.(2.42), the initial state $(\boldsymbol{u}_0, \xi_0, T_0)$ is determined by

$$\begin{cases} \operatorname{div}(-\varepsilon \boldsymbol{C}_0^{-1}\nabla\xi_0) = \rho_e & \text{in } \Omega_R, \\ \xi_0 = 0 & \text{on } \partial\Omega_R, \end{cases} \tag{2.43}$$

and

$$\begin{cases} \operatorname{div}[\mu \boldsymbol{F}_0 - \Pi_0 \boldsymbol{F}_0^{-T} - \dfrac{\varepsilon}{2}|\boldsymbol{F}_0^{-T}\nabla\xi_0|^2 \boldsymbol{F}_0^{-T} \\ \quad + \varepsilon(\boldsymbol{F}_0^{-T}\nabla\xi_0)\otimes(\boldsymbol{C}_0^{-1}\nabla\xi_0)] = 0 & \text{in } \Omega_R, \\ [\mu \boldsymbol{F}_0 - \Pi_0 \boldsymbol{F}_0^{-T} - \dfrac{\varepsilon}{2}|\boldsymbol{F}_0^{-T}\nabla\xi_0|^2 \boldsymbol{F}_0^{-T} \\ \quad + \varepsilon(\boldsymbol{F}_0^{-T}\nabla\xi_0)\otimes(\boldsymbol{C}_0^{-1}\nabla\xi_0)]\boldsymbol{n} = 0 & \text{on } \partial\Omega_R. \end{cases} \tag{2.44}$$

where 0 index denotes the reference state. Upon changing the boundary temperature $T_0 \to T_b$, by Eq.(2.42), the final equilibrium state $(\boldsymbol{u}_f, \xi_f, T_b)$ is determined by

$$\begin{cases} \operatorname{div}(-\varepsilon J \boldsymbol{C}^{-1}\nabla\xi_f) = \rho_e & \text{in } \Omega_R. \\ \xi_f = 0 & \text{on } \partial\Omega_R, \end{cases} \tag{2.45}$$

and

$$\begin{cases} \operatorname{div}[\mu \boldsymbol{F} - \Pi J \boldsymbol{F}^{-T} - \dfrac{\varepsilon}{2} J|\mathbf{F}^{-T}\nabla\xi|^2 \mathbf{F}^{-T} \\ \quad + \varepsilon J(\mathbf{F}^{-T}\nabla\xi)\otimes(\mathbf{C}^{-1}\nabla\xi)] = 0 & \text{in } \Omega_R, \\ [\mu \boldsymbol{F} - \Pi J \boldsymbol{F}^{-T} - \dfrac{\varepsilon}{2} J|\mathbf{F}^{-T}\nabla\xi|^2 \mathbf{F}^{-T} \\ \quad + \varepsilon J(\mathbf{F}^{-T}\nabla\xi)\otimes(\mathbf{C}^{-1}\nabla\xi)]\boldsymbol{n} = 0 & \text{on } \partial\Omega_R. \end{cases} \tag{2.46}$$

where ρ_e represents a surface charge layer as shown in Figure 4, and $\partial\Omega_R$ representing the boundary electrodes. The solution to Eqs. (2.43), (2.44), (2.45), and (2.46) can in general be quite complicated, even for the simple geometry shown in Figure 4. For the film illustrated in Figure 4, we assume that the thickness is much smaller than its width and depth (both are set to be equal). These simplifications ensure that the problem reduces to a 1-dimensional problem and that the deformation and the polarization only depend on the coordinate X and that the polarization is along the X direction throughout the whole process of deformation or application of electric field. Defining stretch in X direction by λ, the stretches in other directions will be $\sqrt{J/\lambda}$. For a traction free

system according to Eqs.(2.46), we have

$$\begin{aligned} \sigma_{xx} &= \mu\lambda - \Pi\frac{J}{\lambda} + \frac{\varepsilon}{2}\frac{J}{\lambda}e^2 = 0, \qquad \text{in } \Omega_R, \\ \sigma_{yy} &= \sigma_{zz} = \mu\sqrt{\frac{J}{\lambda}} - \Pi\sqrt{J\lambda} = 0, \quad \text{in } \Omega_R, \end{aligned} \tag{2.47}$$

where, σ_{ii} denotes the magnitude of stress in i direction and e stands for the magnitude of electric field in current coordinates which is along X direction. Substituting Π from Eq.(2.47)$_2$ to σ_{xx} and choosing the thermoelastic form to be linear: $J = f(T) = 1+3\alpha\Delta T$, where α is the linear thermal expansion coefficient, we have:

$$\sigma_{xx} = \mu(\lambda - \frac{1+3\alpha\Delta T}{\lambda^2}) + \frac{\varepsilon}{2}\frac{(1+3\alpha\Delta T)}{\lambda}e^2 = 0, \quad \text{in } \Omega_R, \tag{2.48}$$

Similarly, for initial state we would have:

$$\sigma_{xx} = \mu(\lambda_0 - \frac{1}{\lambda_0^2}) + \frac{\varepsilon}{2}\frac{1}{\lambda_0}e_0^2 = 0, \quad \text{in } \Omega_R, \tag{2.49}$$

Denoting $\lambda_0 = l_0/L$, we will get:

$$\lambda = \frac{l}{L} = \lambda_0\frac{l}{l_0} \tag{2.50}$$

where $\dfrac{l}{l_0}$ is the stretch caused by temperature change which is $1+\alpha\Delta T$ for linear thermal expansion. Integrating Maxwell equation Eq.(2.8) over the thickness, yields:

$$\begin{cases} 0 - d_1 = q_1 \\ d_2 - 0 = q_2 \\ d_1 - d_2 = q \end{cases} \tag{2.51}$$

where q, q_1, and q_2 are the charge density at the interface, and the induced charge densities in the upper and lower surfaces, respectively. Here, and in what follows, index 1 (resp. 2) correspond to the upper (resp. lower) layer. Since there is no difference in the electric potential on the boundaries, according to the definition of the spatial electric field we have:

$$e_1 l_1 + e_2 l_2 = 0 \tag{2.52}$$

Combining Eqs.(2.51) and (2.52) with the definition of electric displacement ($d_i = \varepsilon_i e_i$), results in

$$q_1 = \frac{-q\varepsilon_1 l_2}{\varepsilon_1 l_2 + \varepsilon_2 l_1}, \qquad q_2 = \frac{-q\varepsilon_2 l_1}{\varepsilon_1 l_2 + \varepsilon_2 l_1} \tag{2.53}$$

$$e_1 = \frac{q l_2}{\varepsilon_1 l_2 + \varepsilon_2 l_1}, \qquad e_2 = \frac{-q l_1}{\varepsilon_1 l_2 + \varepsilon_2 l_1} \tag{2.54}$$

Substituting electric field from Eq.(2.54) and solving Eq.(2.48), we can find the stretches for different directions for each layer. The pyroelectric coefficient can be defined by the variation of induced

electric charge at the electrodes with respect to the temperature difference [NSBG+01]:

$$\begin{aligned} p &= \frac{dq_1}{dT} \\ &= \frac{dq_1}{d\lambda_1}\frac{d\lambda_1}{dT} + \frac{dq_1}{d\lambda_2}\frac{d\lambda_2}{dT} \\ &= \frac{q\frac{\varepsilon_2}{\varepsilon_1}\frac{l_2}{l_1}}{(\frac{\varepsilon_2}{\varepsilon_1}+\frac{l_2}{l_1})^2}(\frac{1}{\lambda_1}\frac{d\lambda_1}{dT} - \frac{1}{\lambda_2}\frac{d\lambda_2}{dT}) \end{aligned} \tag{2.55}$$

For linear thermal expansion condition, $\frac{d\lambda}{dT} = \alpha\lambda_0$. So we have:

$$p = \frac{q\frac{\varepsilon_2}{\varepsilon_1}\frac{l_{0_2}}{l_{0_1}}\frac{1+\alpha_2\Delta T}{1+\alpha_1\Delta T}}{(\frac{\varepsilon_2}{\varepsilon_1}+\frac{l_{0_2}}{l_{0_1}}\frac{1+\alpha_2\Delta T}{1+\alpha_1\Delta T})^2}(\frac{\alpha_1}{1+\alpha_1\Delta T} - \frac{\alpha_2}{1+\alpha_2\Delta T}) \tag{2.56}$$

where $l_0 = L\lambda_0$ and λ_0 is obtained from Eq.(2.49).

The dielectric constant of polymers usually range from 1 to 10, and the thermal expansion coefficients at room temperature are $4 \times 10^{-5}(K^{-1})$ or higher [Ahm12, Sch88]. To present some benchmark results, prior to a discussion on how to maximize pyroelectricity, we choose one layer to be polypropylene polymer foam [NSBG+01], with properties recorded in Table 1, which is a typical material used in electrets and a subject of several of the studies referenced earlier. The emergent pyroelectric coefficient (normalized with respect to the coefficient of the PZT oriented thin films $(3 \times 10^{-4}C/m^2K)$ [SOS+91]) is plotted in Figure 5. The second layer's elastic modulus[6] is set to be $0.7MPa$ for the Figure 5a and the dielectric ratio for Figure 5b is set to be one. Both layers have the same thickness $70\mu m$, a temperature difference of $10°C$ is imposed and the electric charge density at the interface is chosen to be a typical value of $0.002C/m^2$, which is in the same order of magnitude with what Bauer and co-workers [NSBG+01] have indicated in their fabrication of electrets. As evident, and noted in the experiments of Bauer and co-workers [NSBG+01], the pyroelectric effect is rather weak.

Insights into Optimizing Pyroelectricity for Two-Layer Thin Film Electrets

While the benchmark results, in agreement with the limited experimental data, indicate that the pyroelectric response is weak in electrets, we now have the advantage of an explicit analytical expression that may be interrogated to seek guidelines on how to improve this effect. Based on the study of Eq.(2.56), we conclude the following:

[6]The constitutive models for large deformation in soft materials are usually parametrized through the shear modulus. With the realization that some communities are more familiar with the Young's modulus E, we have cited that as key mechanical property in the paper and also later used it in Appendix D in the linearize setting. We remark that E is just a factor of one third of μ for an incompressible material.

Table 1 Material properties of foam PP at room temperature [NSBG+01]

Material property	Polypropylene foam [NSBG+01]
Dielectric constant: $\varepsilon/\varepsilon_0$	1.23
Elastic modulus: E *(MPa)*	2.2
Linear thermal expansion: α (K^{-1})	1.2×10^{-3}

- Increasing the embedded charge: The emergent pyroelectricity depends linearly on the embedded charge. However, there are practical limitations on increasing the charge density and accordingly, this insight may not be of much practical significance.
- Increase of thermal mismatch: the emergent pyroelectric coefficient depends linearly on the thermal mismatch: $\alpha_1 - \alpha_2$ and choosing materials that maximize this will improve the response. We remark that although the pyroelectric coefficient also depends on the applied temperature difference, this effect is almost negligible under nearly all practical situations.
- Thickness ratio: for the structure that we have investigated—a two-layer thin film structure, we arrive at a rather idiosyncratic insight that an optimum pyroelectric coefficient is obtain if the ratio of the dielectric constants of the layers is equal to the ratio of the thickness.
- In contrast to the emergent piezoelectric coefficient of electrets, the effect of layers' elastic modulus is almost negligible for pyroelectricity (Figure 5b).

We utilize the insights recorded in the preceding paragraph in Figure 6 which presents the variation of normalized pyroelectric coefficient with respect to thickness ratios for different ratio of layers' dielectric constant. We set the dielectric constant and thickness of first layer to be $\varepsilon_1 = \varepsilon_0$ and $L_1 = 70\mu m$ respectively; both layers have the same elastic modulus: $1Mpa$, the electric charge density at the interface is set to be $q = 0.002C/m^2$ and the thermal expansion coefficients of layers is set to be $\alpha_1 = 1.2\times10^{-3}K^{-1}$ and $\alpha_2 = 4\times10^{-5}K^{-1}$. Under the most ideal conditions suggested by our interpretation of Eq.(2.56), choosing materials with a high thermal expansion mismatch and large electric charge at the interface can lead to higher pyroelectric response.

2.6 Porous Cellular Polymer Film with Charges Deposited on the Void Surfaces

In this section we derive the response of polymer foam with charges deposited on the upper and lower internal surfaces of the voids. This is the most commonly fabricated and tested configuration in experiments. The voids, that are much softer than the bulk polymer, can be viewed as the second phase of the composite. A triple layered model (shown in Figure 7) is used to approximately mimic the actual system. Past work has shown that this simplified model replacement works quite well to capture the response of the emergent piezoelectricity of the electret foams [DLS14].

Integrating Maxwell equation Eq.(2.8) over the thickness, yields:

$$\begin{cases} 0 - d_1 = q_1 \\ d_1 - d_2 = -q_0 \\ d_2 - d_3 = q_0 \\ d_3 - 0 = q_2 \end{cases} \tag{2.57}$$

where q_0 (resp. $-q_0$) is the charge density on the upper (resp. lower) internal surface, q_1 (resp. q_2) is the induced charge density on the upper (resp. lower) electrode, and d_1, d_2, and d_3 are the electric displacements of upper layer, void, and lower layer respectively.

2.7 Pyroelectric coefficient for the foam electret

For short-circuit boundary conditions, we have:

$$2V_p + V_a = 0 \tag{2.58}$$

Here and in what follows, subscripts a and p stand for void and polymer respectively. This results in

$$e_a = \frac{q_0 h_p}{\varepsilon_0 h_p + \varepsilon_p h_a}, \qquad e_p = \frac{-q_0 h_a}{\varepsilon_0 h_p + \varepsilon_p h_a} \tag{2.59}$$

and

$$q_1 = -q_2 = \frac{\varepsilon_p q_0 h_a}{\varepsilon_0 h_p + \varepsilon_p h_a} \tag{2.60}$$

The pyroelectric coefficient is then obtained as:

$$\begin{aligned} p &= \frac{dq_1}{dT} \\ &= \frac{dq_1}{d\lambda_a}\frac{d\lambda_a}{dT} + \frac{dq_1}{d\lambda_p}\frac{d\lambda_p}{dT} \\ &= \frac{\frac{\varepsilon_p}{\varepsilon_a} q_0 H_a H_p}{(\lambda_p H_p + \frac{\varepsilon_p}{\varepsilon_a}\lambda_a H_a)^2}(\lambda_p \lambda_a' - \lambda_a \lambda_p') \end{aligned} \tag{2.61}$$

where H denotes the reference thickness (before applying temperature difference), λ is the stretch, and $'$ denotes differentiation with respect to temperature. Substituting $\lambda_a = 1 + \alpha_a \Delta T$, $\lambda_p = 1 + \alpha_p \Delta T$, $\lambda_a' = \alpha_a$ and $\lambda_p' = \alpha_p$, we have[7]

$$p = q_0 \frac{\varepsilon_p}{\varepsilon_a}\frac{H_p}{H_a}\frac{\big(\alpha_a(1+\alpha_p\Delta T) - \alpha_p(1+\alpha_a\Delta T)\big)}{\big(\frac{H_p}{H_a}(1+\alpha_p\Delta T) + \frac{\varepsilon_p}{\varepsilon_a}(1+\alpha_a\Delta T)\big)^2} \tag{2.62}$$

[7]The difference between this kind of electret and two-layer electret is that here the reference dimensions are already known and there is no need to use Eq.(2.42) to find the reference stretches.

In the experimental work [NSBG+01], the precise temperature at which the measurements were carried out was not indicated (although we speculate that it was around room temperature). Furthermore, the precise charge density in the experiments is also not known (although, again, based on the emergent piezoelectric response, an approximate range can be estimated). Accordingly, in order to compare our predictions with experiments, in Figure 8, we show the emergent pyroelectric coefficient of the porous electret with respect to the likely range of charge density at the interface. Furthermore, we assume that the void is an ideal gas at atmospheric pressure and $T = 25°C$, $\varepsilon_p = 2.2\varepsilon_0$, $H_a = 44\mu m$, and $H_p = 26\mu m$. Given these assumptions, our model provides reasonably encompasses the experimental observation by Neugschwandtner, et al [NSBG+01].

With the limited experimental validation at hand, and using the insights recorded earlier, we can now consider optimizing and designing a larger pyroelectric response than what has been demonstrated experimentally. Using the polymer property ranges stated in Section 2.5, Figure 9 shows how our model can be used to improve the pyroelectric response by one order of magnitude over the experiments by Neugschwandtner, et al [NSBG+01].

2.8 Emergent Electrocaloric Behavior

To investigate the emergent electrocaloric behavior, we apply a voltage difference to the adiabatic boundaries of the structure considered in the previous section—shown in Figure 10. We assume that the system is initially maintained at zero voltage difference (i.e., short circuit) and a constant temperature T_0 without external body force and traction. By Eq.(2.42), the initial state $(\boldsymbol{u}_0, \xi_0, T_0)$ is determined by

$$\begin{cases} \operatorname{div}[\mu \boldsymbol{F}_0 - \Pi_0 \boldsymbol{F}_0^{-T} - \dfrac{\varepsilon}{2}|\mathbf{F}_0^{-T}\nabla\xi_0|^2\mathbf{F}_0^{-T} \\ \quad + (\mathbf{F}_0^{-T}\nabla\xi_0)\otimes(\varepsilon\mathbf{C}_0^{-1}\nabla\xi_0)] = 0 & \text{in } \Omega_R, \\ [\mu \boldsymbol{F}_0 - \Pi_0 \boldsymbol{F}_0^{-T} - \dfrac{\varepsilon}{2}|\mathbf{F}_0^{-T}\nabla\xi_0|^2\mathbf{F}_0^{-T} \\ \quad + (\mathbf{F}_0^{-T}\nabla\xi_0)\otimes(\varepsilon\mathbf{C}_0^{-1}\nabla\xi_0)]\boldsymbol{n} = 0 & \text{on } \partial\Omega_R, \\ \operatorname{div}(-\varepsilon\mathbf{C}_0^{-1}\nabla\xi_0) = \rho_e & \text{in } \Omega_R, \\ \xi_0 = 0 & \text{on } \{X = -L_2 \text{ or } L_1\}. \end{cases} \tag{2.63}$$

Upon applying a potential difference such that

$$V_1 - V_2 = V, \tag{2.64}$$

we denote the final equilibrium state by $(\boldsymbol{u}_f, \xi_f, T_f)$. Again, by Eq.(2.42) the final state satisfies

$$\begin{cases} \operatorname{div}[\mu \boldsymbol{F}_f - \Pi_f J \boldsymbol{F}_f^{-T} - \dfrac{\varepsilon}{2} J |\mathbf{F}_f^{-T} \nabla \xi_f|^2 \mathbf{F}_f^{-T} \\ \quad + (\mathbf{F}_f^{-T} \nabla \xi_f) \otimes (\varepsilon J \mathbf{C}_f^{-1} \nabla \xi_f)] = 0 & \text{in } \Omega_R, \\ [\mu \boldsymbol{F}_f - \Pi_f J \boldsymbol{F}_f^{-T} - \dfrac{\varepsilon}{2} J |\mathbf{F}_f^{-T} \nabla \xi_f|^2 \mathbf{F}_f^{-T} \\ \quad + (\mathbf{F}_f^{-T} \nabla \xi_f) \otimes (\varepsilon J \mathbf{C}_f^{-1} \nabla \xi_f)] \boldsymbol{n} = 0 & \text{on } \partial\Omega_R, \\ \operatorname{div}(-\varepsilon J \mathbf{C}_f^{-1} \nabla \xi_f) = \rho_e & \text{in } \Omega_R, \\ \xi_f = V_1 \text{ (resp. } V_2) & \text{on } \{X = L_1\} (\text{resp. } \{X = -L_2\}). \end{cases} \tag{2.65}$$

where ρ_e represents a surface charge layer as shown in Figure 10 and 0 (resp. f) index corresponds to initial (resp. final) state. We remark that the final state is completely determined by Eq.(2.65) once the final temperature T_f is determined. To determine the final temperature in this process, by the first law of thermodynamics we have

$$U_f - U_0 = W^e, \tag{2.66}$$

where U is the internal energy of the system, and W^e is the total work done to the system which, by Eq.(2.15), can be written as

$$W^e = \int P_{\text{ext}} dt = \int_{\Omega_R} \varepsilon \nabla \xi_f \cdot (J \boldsymbol{C}_f^{-1} \nabla \xi_f - \boldsymbol{C}_0^{-1} \nabla \xi_0). \tag{2.67}$$

In addition, from Eqs.(2.3), (2.37), and (2.38) we find that

$$S(\boldsymbol{F}, \boldsymbol{P}, T) = C(\log T/T_0 + 1) + 3\Pi\alpha, \tag{2.68}$$

and hence, taking into account Eq.(2.4), the internal energy density Φ can be written as

$$\Phi(\boldsymbol{F}, \boldsymbol{P}, T) = \Psi_0 + CT + \frac{\mu}{2}(I_1 - 3) + \Pi|J - 1 + 3\alpha T_0| + \frac{a}{2J}|\boldsymbol{P}|^2.$$

Therefore, by Eq.(2.5) we find that

$$\begin{aligned} U_f - U_0 = \int_{\Omega_R} \Big[& C(T_f - T_0) + \frac{\mu}{2}(I_{1_f} - I_{1_0}) + \Pi|J - 1 + 3\alpha T_0| \\ & - \Pi_0(3\alpha T_0) + \frac{\varepsilon}{2}(J|\boldsymbol{F}_f^{-T} \nabla \xi_f|^2 - |\boldsymbol{F}_0^{-T} \nabla \xi_0|^2) \Big]. \end{aligned} \tag{2.69}$$

Inserting Eqs.(2.67) and (2.69) into Eq.(2.66), we have

$$\begin{aligned} U_f - U_0 - W^e = \int_{\Omega_R} \Big[& C(T_f - T_0) + \frac{\mu}{2}(I_{1_f} - I_{1_0}) + \Pi|J - 1 + 3\alpha T_0| \\ & - \Pi_0(3\alpha T_0) + \frac{\varepsilon}{2}(J|\boldsymbol{F}_f^{-T} \nabla \xi_f|^2 - |\boldsymbol{F}_0^{-T} \nabla \xi_0|^2) \\ & - \varepsilon \nabla \xi_f \cdot (J \boldsymbol{C}_f^{-1} \nabla \xi_f - \boldsymbol{C}_0^{-1} \nabla \xi_0) \Big] = 0. \end{aligned} \tag{2.70}$$

The final temperature T_f can be determined by solving Eq.(2.70) together with Eq.(2.65). Again assuming that the deformation and the polarization only depend on the coordinate X, polarization is along the X direction and defining the stretch in X direction by λ, for the simple case shown in Figure 10, Eq.(2.52) changes to: $e_1 l_1 + e_2 l_2 = -V$. Combining with Eq.(2.51) we obtain:

$$q_1 = \frac{-q\varepsilon_1 l_2 + \varepsilon_1\varepsilon_2 V}{\varepsilon_1 l_2 + \varepsilon_2 l_1}, \qquad q_2 = \frac{-q\varepsilon_2 l_1 - \varepsilon_1\varepsilon_2 V}{\varepsilon_1 l_2 + \varepsilon_2 l_1} \tag{2.71}$$

$$e_1 = \frac{q l_2 - \varepsilon_2 V}{\varepsilon_1 l_2 + \varepsilon_2 l_1}, \qquad e_2 = \frac{-q l_1 - \varepsilon_1 V}{\varepsilon_1 l_2 + \varepsilon_2 l_1} \tag{2.72}$$

Eq.(2.48) together with Eq.(2.70) and the substitution of $\Pi_0 = \mu/\lambda_0$ and $\Pi = \mu/\lambda$ for the case that layers' width in directions other than X are the same, yields

$$\mu_1(\lambda_{0_1} - \frac{1}{\lambda_{0_1}^2}) + \frac{\varepsilon_1}{2}\frac{1}{\lambda_{0_1}} e_{0_1}^2 = 0 \tag{2.73a}$$

$$\mu_2(\lambda_{0_2} - \frac{1}{\lambda_{0_2}^2}) + \frac{\varepsilon_2}{2}\frac{1}{\lambda_{0_2}} e_{0_2}^2 = 0 \tag{2.73b}$$

$$\mu_1(\lambda_1 - \frac{1+3\alpha_1\Delta T}{\lambda_1^2}) + \frac{\varepsilon_1}{2}\frac{1+3\alpha_1\Delta T}{\lambda_1} e_1^2 = 0, \tag{2.73c}$$

$$\mu_2(\lambda_2 - \frac{1+3\alpha_2\Delta T}{\lambda_2^2}) + \frac{\varepsilon_2}{2}\frac{1+3\alpha_2\Delta T}{\lambda_2} e_2^2 = 0, \tag{2.73d}$$

$$C_1 L_1 \Delta T + \frac{\mu_1 L_1}{2}(\lambda_1^2 + \frac{2(1+3\alpha_1\Delta T)}{\lambda_1} - \lambda_{0_1}^2 - \frac{2}{\lambda_{0_1}}) \tag{2.73e}$$

$$\begin{aligned}
&+C_2 L_2 \Delta T + \frac{\mu_2 L_2}{2}(\lambda_2^2 + \frac{2(1+3\alpha_2\Delta T)}{\lambda_2} - \lambda_{0_2}^2 - \frac{2}{\lambda_{0_2}}) \\
&-\frac{\varepsilon_1}{2} L_1 \big(e_{0_1}^2 - 2\frac{\lambda_1}{\lambda_{0_1}} e_1 \cdot e_{0_1} + (1+3\alpha_1\Delta T) e_1^2\big) \\
&-\frac{\varepsilon_2}{2} L_2 \big(e_{0_2}^2 - 2\frac{\lambda_2}{\lambda_{0_2}} e_2 \cdot e_{0_2} + (1+3\alpha_2\Delta T) e_2^2\big) \\
&+3\alpha_1\mu_1 L_1(\frac{T_f}{\lambda_1} - \frac{T_0}{\lambda_{0_1}}) + 3\alpha_2\mu_2 L_2(\frac{T_f}{\lambda_2} - \frac{T_0}{\lambda_{0_2}}) = 0
\end{aligned}$$

where e_{1_0} (resp. e_{2_0}) represents the electric field in reference configuration across layer 1 (resp. layer 2) when the applied voltage to the whole system is zero and ΔT denotes the temperature change. Solving the nonlinear set of equations Eqs.(2.73), we can find the unknowns: λ_{0_1}, λ_{0_2}, λ_1, λ_2, and T_f.

In order to obtain a simple closed-form expression to illustrate the basic form of the solution, an analytical solution may be derived for a linearized model. The derivation of the linearized model is

Table 2 Material properties of polyproplene (PP) and polyethylene (PE) at room temperature

Material property	PP	PE
Dielectric constant $\varepsilon/\varepsilon_0$ [Ahm12, SCB10]	2.2	2.3
Elastic modulus E (GPa) [GS98]	1.09	1.6
Mass density ρ (kg/m^3) [PJK59, BIG$^+$89]	905	940
Specific heat C (J /kg K) [AC93]	1900	1800
Thermal expansion α (K^{-1}) [KFRP08, BIG$^+$89]	10^{-4}	2.48×10^{-4}

recorded in Appendix D, and the final answer (temperature change) with that assumption is:

$$T_f - T_0 = \frac{\frac{\varepsilon_1}{2L_1}V_1^2 + \frac{\varepsilon_2}{2L_2}V_2^2}{C_1L_1 + C_2L_2 + (\alpha_1^2 E_1 L_1 + \alpha_2^2 E_2 L_2)T_0} \tag{2.74}$$

where V_1 (resp. V_2) denotes the voltage difference across the 1^{st} (resp. 2^{nd}) layer. To generate numerical results, we assume that the two layers be polyethylene and polyproplene, with material properties given in table 2 and the electric charge density at the interface is assumed to be $0.001C/m^2$. The temperature change of electret with respect to voltage applied to the system for both linear and nonlinear solution are presented in Figure 11.

As evident in Figure 11, the linearized approximation adequately captures the nonlinear numerical predictions, which is large enough compared to other electrocaloric materials [Val12]. The two insights from Eq.(2.74) are as follows:

- Using materials with lower specific heat will lead to a stronger electrocaloric effect.
- The effect of mechanical properties, charge density and thermal expansion is weaker in the case of electrocaloric effect (as opposed to pyroelectricity) but in general, softer is better and a smaller thermal coefficient favors a stronger electrocaloric effect.

2.9 Porous Cellular Polymer Film with Charges Deposited on the Void Surfaces

By applying potential difference of V to the electret shown in Figure 7, we have

$$2V_p + V_a = -V \tag{2.75}$$

and

$$e_a = \frac{q_0 h_p + \varepsilon_p V}{\varepsilon_0 h_p + \varepsilon_p h_a} \qquad \textit{and} \qquad e_p = \frac{-q_0 h_a + \varepsilon_0 V}{\varepsilon_0 h_p + \varepsilon_p h_a} \tag{2.76}$$

Pursuing the same procedure as Eq.(2.73), we obtain[8]

$$\frac{H_a}{H_p+H_a}\mu(\lambda_{0_a}-\frac{1}{\lambda_{0_a}^2})+\frac{\varepsilon_0}{2}\frac{1}{\lambda_{0_a}}e_{0_a}^2=0 \tag{2.79a}$$

$$\mu_p(\lambda_{0_p}-\frac{1}{\lambda_{0_p}^2})+\frac{\varepsilon_p}{2}\frac{1}{\lambda_{0_p}}e_{0_p}^2=0 \tag{2.79b}$$

$$\frac{H_a}{H_p+H_a}\mu(\lambda_a-\frac{1+3\alpha_a\Delta T}{\lambda_a^2})+\frac{\varepsilon_0}{2}\frac{1+3\alpha_a\Delta T}{\lambda_a}e_a^2=0, \tag{2.79c}$$

$$\mu_p(\lambda_p-\frac{1+3\alpha_p\Delta T}{\lambda_p^2})+\frac{\varepsilon_p}{2}\frac{1+3\alpha_p\Delta T}{\lambda_p}e_p^2=0, \tag{2.79d}$$

$$\frac{H_a^2}{2(H_p+H_a)}\mu(\lambda_a^2+\frac{2(1+3\alpha_a\Delta T)}{\lambda_a}-\lambda_{0_a}^2-\frac{2}{\lambda_{0_a}}) \tag{2.79e}$$

$$\begin{aligned}
&-\frac{\varepsilon_0}{2}H_a\big(e_{0_a}^2-2\frac{\lambda_a}{\lambda_{0_a}}e_a\cdot e_{0_a}+(1+3\alpha_a\Delta T)e_a^2\big)+(C_aH_a+C_pH_p)\Delta T\\
&+\frac{\mu_pH_p}{2}(\lambda_p^2+\frac{2(1+3\alpha_p\Delta T)}{\lambda_p}-\lambda_{0_p}^2-\frac{2}{\lambda_{0_p}})\\
&+3(\alpha_p\mu_pH_p+\alpha_a\frac{H_a^2\mu}{H_p+H_a})(\frac{T_f}{\lambda_a}-\frac{T_0}{\lambda_{0_a}})\\
&-\frac{\varepsilon_p}{2}H_p\big(e_{0_p}^2-2\frac{\lambda_p}{\lambda_{0_p}}e_p\cdot e_{0_p}+(1+3\alpha_p\Delta T)e_p^2\big)=0
\end{aligned}$$

We considered void specific heat as $C_a=1KJ/KgK$ and based on experimental data reported in [DLS14], we set average elastic modulus to be $E=0.8MPa$, $H_a=38\mu m$, $H_p=32\mu m$, $q_0=0.001C/m2$, and $\varepsilon_p=2.35\varepsilon_0$. Figure 12 shows the variation of temperature difference with respect to voltage difference applied to the foam electret.

[8]Since the average Young's modulus of the whole structure is much lower than the polymer without void, it is reasonable to assume that the deformation in the polymer layers is negligible in comparison to the pores [DLS14] (and $\lambda_p=1+\alpha_p\Delta T\approx 1$). Then, for the stress–free boundary condition, we will have

$$\sigma_x=\frac{H_a}{H_p+H_a}\mu(\lambda_a-\frac{1+3\alpha_a\Delta T}{\lambda_a^2})+\frac{\varepsilon_0}{2}\frac{(1+3\alpha_a\Delta T)}{\lambda_a}e_a^2=0 \tag{2.77}$$

And Eq.(2.70) will simplify to

$$\begin{aligned}
&\big(C_aH_a+C_pH_p\big)\Delta T+\frac{H_a^2\mu}{2(H_p+H_a)}(\lambda_a^2+\frac{2(1+3\alpha_a\Delta T)}{\lambda_a}-3)+6\mu_pH_p\alpha_p\Delta T\\
&+3\alpha_a\frac{H_a^2\mu}{H_p+H_a}(\frac{T_f}{\lambda_a}-T_0)-\frac{\varepsilon_a}{2}H_a\big(e_{0_a}^2-2\lambda_ae_a\cdot e_{0_a}+(1+3\alpha_a\Delta T)e_a^2\big)\\
&-\frac{\varepsilon_p}{2}H_p\big(e_{0_p}^2-2e_p\cdot e_{0_p}+(1+3\alpha_p\Delta T)e_p^2\big)=0
\end{aligned} \tag{2.78}$$

where μ is the average shear modulus of the foam. Solving Eq.(2.77) together with Eq.(2.78), we will get the two unknowns: λ_a and ΔT.

3 Concluding Remarks

Soft pyroelectrics and electrocaloric materials are not readily available. The most common pyroelectric materials are hard crystalline ceramics or at best weakly responsive polymers like PVDF. In this work, we have created a general framework to model emergent pyroelectricity and electrocaloric behavior in electrets. Using a simplified illustrative model of a layered as well as foam electrets, we have presented several insights into how soft pyroelectric and electrocaloric materials may be designed. Specifically, we are able to validate our model with respect to the limited experimental data available in the literature as well as design an order of magnitude larger pyroelectric response than what has been obtained so far. In addition, a non-trivial electrocaloric effect is predicted for the first time in the context of soft electrets.

Acknowledgements

P.S. would like to gratefully acknowledge support from the M. D. Anderson Professorship of the University of Houston and NSF CMMI grant 1463205. L. L. gratefully acknowledges the support of NSF CMMI-135156, DMS-1410273, NSFC-1152800009, and AFOSR-FA9550-16-1-0181. Kaushik Dayal acknowledges support from NSF Mechanics of Materials and Structures (1150002 and 1635407), NSF Manufacturing Machines and Equipment (1635435), ARO Numerical Analysis (W911NF-17-1-0084), and ONR Applied and Computational Analysis (N00014-18-1-2528)

Appendices

A Calculation of $\frac{d}{dt}\mathcal{E}$

First, by the chain rule we find that

$$\begin{aligned}
&\frac{d}{dt}\boldsymbol{F}^{-1} = -\boldsymbol{F}^{-1}\dot{\boldsymbol{F}}\boldsymbol{F}^{-1},\\
&\dot{J} = J\mathrm{Tr}(\boldsymbol{F}^{-1}\dot{\boldsymbol{F}}) = J\boldsymbol{F}^{-T}\cdot\dot{\boldsymbol{F}},\\
&\frac{d}{dt}(J\boldsymbol{C}^{-1}) = -J\boldsymbol{F}^{-1}\dot{\boldsymbol{F}}\boldsymbol{C}^{-1}\\
&\qquad - J\boldsymbol{C}^{-1}\dot{\boldsymbol{F}}^{T}\boldsymbol{F}^{-T} + J(\boldsymbol{F}^{-T}\cdot\dot{\boldsymbol{F}})\boldsymbol{C}^{-1},
\end{aligned} \tag{A.1}$$

and hence

$$\begin{aligned}
\frac{\epsilon_0}{2}\nabla\xi\cdot\overline{J\boldsymbol{C}^{-1}}\nabla\xi = -\epsilon_0 J\dot{\boldsymbol{F}}\cdot\big[&(\mathbf{F}^{-T}\nabla\xi)\otimes(\mathbf{C}^{-1}\nabla\xi)\\
&-\frac{1}{2}|\mathbf{F}^{-T}\nabla\xi|^2\mathbf{F}^{-T}\big].
\end{aligned} \tag{A.2}$$

Therefore,

$$\begin{aligned}\frac{d}{dt}[\frac{\epsilon_0}{2}\nabla\xi\cdot J\boldsymbol{C}^{-1}\nabla\xi] &= \frac{\epsilon_0}{2}\dot{\overline{\nabla\xi}}\cdot J\boldsymbol{C}^{-1}\nabla\xi+\frac{\epsilon_0}{2}\nabla\xi\cdot\frac{d}{dt}[J\boldsymbol{C}^{-1}\nabla\xi]\\ &= \frac{\epsilon_0}{2}\dot{\overline{\nabla\xi}}\cdot J\boldsymbol{C}^{-1}\nabla\xi+\frac{\nabla\xi}{2}\cdot(-\dot{\boldsymbol{D}}+\dot{\overline{\boldsymbol{F}^{-1}\boldsymbol{P}}})\\ &= \boldsymbol{\Sigma}_{\rm MW}\cdot\dot{\boldsymbol{F}}+\nabla\xi\cdot\boldsymbol{F}^{-1}\dot{\boldsymbol{P}}-\nabla\xi\cdot\dot{\boldsymbol{D}},\end{aligned}$$

By the divergence theorem, we conclude that

$$\frac{d}{dt}\mathcal{E}=\int_{\Omega_R}[\boldsymbol{\Sigma}_{\rm MW}\cdot\dot{\boldsymbol{F}}+(\boldsymbol{F}^{-T}\nabla\xi)\cdot\dot{\boldsymbol{P}}+\xi{\rm div}\dot{\boldsymbol{D}}]-\int_{\partial\Omega_R}\xi\dot{\boldsymbol{D}}\cdot\boldsymbol{n}. \tag{A.3}$$

B More general dissipation mechanisms

Our framework can be used to address broad non-equilibrium processes upon postulating more general dissipation function. For example, to address the energy dissipation associated with viscosity and evolution of polarization, we may postulate that ($\boldsymbol{g}=\nabla T$)

$$\Gamma=\Gamma_0(\boldsymbol{g},\boldsymbol{F},\boldsymbol{P},T)+\Gamma_1(\dot{\boldsymbol{F}},\boldsymbol{F},\boldsymbol{P},T)+\Gamma_2(\dot{\boldsymbol{P}},\boldsymbol{F},\boldsymbol{P},T),$$

and that Γ_i ($i=0,1,2$) are *analytic* functions with respect ot their first argument and satisfy

$$\Gamma_i(\cdot,\boldsymbol{F},\boldsymbol{P},T)\geq\Gamma_i(0,\boldsymbol{F},\boldsymbol{P},T)=0.$$

Since $(\cdot)\mapsto\Gamma_i(\cdot,\boldsymbol{F},\boldsymbol{P},T)$ is analytic, we can always rewrite it as

$$\Gamma_0(\boldsymbol{g},\boldsymbol{F},\boldsymbol{P},T)=\boldsymbol{g}\cdot\boldsymbol{\Sigma}_{\boldsymbol{g}}(\boldsymbol{g},\boldsymbol{F},\boldsymbol{P},T),$$

where $\boldsymbol{\Sigma}_{\boldsymbol{m}}$ may be referred to as the *dissipative* force associated with the particular dissipation mechanism (due to the quantity $\boldsymbol{m}$). Then by Eq. (2.22) and in parallel to Eq. (2.26), we have

$$\begin{aligned}\int_{\Omega_R}\Big[&-({\rm div}\boldsymbol{\Sigma}_{\rm tot}+\boldsymbol{b}_e)\cdot\dot{\boldsymbol{x}}+(\frac{\partial\Psi}{\partial\mathbf{P}}+\mathbf{F}^{-T}\nabla\xi-\boldsymbol{\Sigma}_{\dot{\boldsymbol{P}}})\cdot\dot{\mathbf{P}}\\ &-(\Gamma_0+\frac{1}{T}\mathbf{q}\cdot\nabla T)\Big]+\int_{\partial\Omega_R}(\boldsymbol{\Sigma}_{\rm tot}\boldsymbol{n}-\mathbf{t}_e)\cdot\dot{\mathbf{u}}_b=0,\end{aligned} \tag{B.1}$$

where

$$\boldsymbol{\Sigma}_{\rm tot}=\frac{\partial\Psi}{\partial\boldsymbol{F}}+\boldsymbol{\Sigma}_{\rm MW}+\boldsymbol{\Sigma}_{\dot{\boldsymbol{F}}}$$

is the total stress including the contribution from the viscosity. We now repeat the argument from Eq. (2.25) to Eq. (2.30), and conclude the following local equations:

$$\begin{cases}{\rm div}\boldsymbol{\Sigma}_{\rm tot}=-\boldsymbol{b}_e & \text{in } \Omega_R,\\ \dfrac{\partial\Psi}{\partial\mathbf{P}}+\mathbf{F}^{-T}\nabla\xi-\boldsymbol{\Sigma}_{\dot{\boldsymbol{P}}}=0 & \text{in } \Omega_R,\\ -T\dfrac{d}{dt}\dfrac{\partial\Psi}{\partial T}-r_e+{\rm div}\boldsymbol{q}=0,\quad \boldsymbol{q}=-T\boldsymbol{\Sigma}_{\boldsymbol{g}} & \text{in } \Omega_R.\end{cases} \tag{B.2}$$

From (B.2), we see that the physical model for the system is completely prescribed once we specify the free energy function Ψ and dissipation function Γ. We have seen one example of such a model concerning the coupling of elasticity, electrostatics and thermal transport (cf., Eqs. (2.37) and (2.39)). The reader is invited to verify that several well-known dissipative models may be recovered from these equations e.g. the classical Stokes flow for incompressible fluid. We give here a simple example related to micromagnetics. In the absence of elasticity ($\nabla \boldsymbol{x} \equiv \boldsymbol{I}$) and setting

$$\Psi = a_{\text{ex}}|\nabla \boldsymbol{P}|^2 + \phi_{\text{an}}(\boldsymbol{P}) + K(|\boldsymbol{P}| - 1)^2,$$
$$\Gamma_0 = \Gamma_1 = 0, \quad \Gamma_2 = \kappa|\dot{\boldsymbol{P}}|^2,$$

then in the limit $K \to +\infty$, we should impose the constraint $\boldsymbol{P} = 1$ and $(\text{B.2})_2$ should be replaced by

$$\boldsymbol{P} \times (-\boldsymbol{E}_{\text{eff}} + \kappa \dot{\boldsymbol{P}}) = 0, \tag{B.3}$$

where $\boldsymbol{E}_{\text{eff}} = a_{\text{ex}} \Delta \boldsymbol{P} - \nabla \xi - \frac{\partial}{\partial \boldsymbol{P}} \phi_{\text{an}}(\boldsymbol{P})$. In addition, taking into account of the kinetic energy and in the context of micromagnetics, Eq. (B.3) recovers the Landau-Lifshitz-Gilbert equation describing the relaxation of Larmor precession of the magnetization [Bro63].

C Extension of the Model to Account for Stray Electric Fields Outside the Specimen

Many geometries of practical interest, e.g. parallel plate or interdigitated electrodes, leave exposed part of the boundary of the specimen. Since vacuum is also a dielectric medium, the exposed surfaces allow so-called stray electric fields to be present in vacuum. As the vacuum fields contain energy, it can be important to account for them. We briefly describe the extension of the model to this setting.

The starting point is that the electrical energy $\mathcal{E}$ in Eq.(2.10) now uses an integration over all of space rather than only the specimen Ω_t:

$$\mathcal{E}[\boldsymbol{x}, \boldsymbol{P}] = \int_{\mathbb{R}^3} \frac{\epsilon_0}{2} |\nabla_{\boldsymbol{x}} \xi|^2 \tag{C.1}$$

Along with this, the electrostatic Gauss equation governing the electric field is also posed on all of space, i.e., Eq.(2.8) now reads:

$$\text{div}_{\boldsymbol{x}}(-\epsilon_0 \nabla_{\boldsymbol{x}} \xi + \boldsymbol{P}/J) = \rho_e/J \qquad \text{in } \mathbb{R}^3 \tag{C.2}$$

The quantities $\boldsymbol{P}$ and ρ_e are defined only on Ω_R and are set to 0 in vacuum. The typical boundary conditions in all of space, the interface conditions on the surface of the body exposed to vacuum, and efficient ways to solve the electrostatic Gauss equation in all of space, are discussed in, e.g. [YD11, DB07].

We can follow very closely the approach described in [Jam02] to find the resulting field equations. The resulting equations differ from Eq.(2.42) only in that Eq.(2.42)$_2$ will now be posed over all of space with the appropriate boundary and interface conditions, and that ϵ in there will be a function of position: $\epsilon = \epsilon_0$ in vacuum.

D Linearized electrocaloric behavior

In the regime of small strain and moderately small electric field in the sense that $\boldsymbol{H} := \boldsymbol{F} - \boldsymbol{I}$.

$$|\boldsymbol{H}| \sim |\frac{\boldsymbol{P}}{P_s}|^2 \sim \eta \ll 1, \tag{D.1}$$

where P_s is some benchmark polarization for nondimensionalization. Then the constitutive behaviors of the body can be well captured by expanding the free energy function Ψ with respect to $(\boldsymbol{F}, \boldsymbol{P})$ and truncating at $O(\eta^2)$-terms:

$$\begin{aligned}\Psi(\boldsymbol{F}, \mathbf{P}, T) = \Psi(\boldsymbol{I}, 0, T) - (T - T_0)\boldsymbol{\beta} \cdot \boldsymbol{H} + \frac{1}{2}\boldsymbol{H} \cdot \mathbb{C}\boldsymbol{H} \\ + \frac{1}{2}\boldsymbol{P} \cdot \boldsymbol{\chi}\boldsymbol{P} + \boldsymbol{H} \cdot \mathbb{M}(\boldsymbol{P} \otimes \boldsymbol{P}),\end{aligned} \tag{D.2}$$

where (all derivatives are evaluated at $(\boldsymbol{F}, \boldsymbol{P}, T) = (\boldsymbol{I}, 0, T)$)

$$\boldsymbol{\beta} = \frac{\partial \Psi}{\partial \boldsymbol{F}}, \quad \mathbb{C} = \frac{\partial^2 \Psi}{\partial \boldsymbol{F} \partial \boldsymbol{F}}, \quad \boldsymbol{\chi} = \frac{\partial^2 \Psi}{\partial \boldsymbol{P} \partial \boldsymbol{P}}, \quad \mathbb{M} = \frac{1}{2}\frac{\partial^3 \Psi}{\partial \boldsymbol{F} \partial \boldsymbol{P} \partial \boldsymbol{P}}, \tag{D.3}$$

and the $\boldsymbol{P} \cdot \dfrac{\partial \Psi}{\partial \boldsymbol{P}}$ and $\boldsymbol{F} \cdot (\dfrac{\partial^2 \Psi}{\partial \boldsymbol{F} \partial \boldsymbol{P}})\boldsymbol{P}$ terms have to vanish in the expansion (D.2) because of isotropy. $\Psi(\boldsymbol{I}, 0, T) = \Psi_0 - CT \log T/T_0$. Also, we identify $\mathbb{C}$ as the fourth-order elasticity tensor, $\boldsymbol{\chi}$ the second-order susceptibility tensor, $\boldsymbol{\beta}$ the second-order tensor related with thermal stress/strain, $\mathbb{M}$ the fourth-order electrostriction tensor. Since the material is isotropic, by Eqs.(2.32) and (2.33) we infer that all second-order tensors have to be proportional to the identity tensor:

$$(\boldsymbol{\chi}, \boldsymbol{\beta}) = (\chi, \hat{\beta})\boldsymbol{I}, \tag{D.4}$$

and the fourth-order tensors $\mathbb{C}, \mathbb{M}$ has to satisfy that for any $(\boldsymbol{H}, \boldsymbol{P}) \in \mathbb{R}^{3\times 3} \times \mathbb{R}^3$,

$$\begin{aligned}\mathbb{C}\boldsymbol{H} &= \mu(\boldsymbol{H} + \boldsymbol{H}^T) + \lambda(\mathrm{Tr}\boldsymbol{H})\boldsymbol{I}, \\ \mathbb{M}(\boldsymbol{P} \otimes \boldsymbol{P}) &= -\frac{1}{2}\chi|\boldsymbol{P}|^2\boldsymbol{I},\end{aligned} \tag{D.5}$$

where μ, λ are the familiar Lamé constants, and the second equation follows from the assumption that the dielectric constant is independent of deformation gradient (see Remark 2, Liu and Sharma [LS18]). With the same assumptions as brought in section 2 and keeping only the leading order terms in Eq.(2.31), by (D.1) we obtain the governing equation for $(\boldsymbol{u}, \xi, T)$:

$$\begin{cases} \mathrm{div}[\mathbb{C}\nabla\boldsymbol{u} + \hat{\beta}\triangle T\boldsymbol{I} + \dfrac{\varepsilon}{2}\mathbb{T}(\nabla\xi \otimes \nabla\xi)] = -\boldsymbol{b}_e & \text{in } \Omega_R, \\ \mathrm{div}(-\varepsilon\nabla\xi) = \rho_e & \text{in } \Omega_R, \\ C\dot{T} + T\hat{\beta}\mathrm{div}\dot{\boldsymbol{u}} = r_e + \mathrm{div}(k\nabla T) & \text{in } \Omega_R, \end{cases} \tag{D.6}$$

where the fourth-order tensor $\mathbb{T}$ is the special case of $\mathbb{C}$ in (D.5) with $\mu = \lambda = 1$. The reader is referred to Liu and Sharma [LS18] for more technical details.

For electrocaloric response, assume the system is initially maintained at zero voltage difference (i.e., short circuit) and a constant temperature T_0 without external body force and traction. By (D.6), the initial state $(\boldsymbol{u}_0, \xi_0, T_0)$ is determined by

$$\begin{cases} \operatorname{div}[\mathbb{C}\nabla \boldsymbol{u}_0 + \dfrac{\varepsilon}{2}\mathbb{T}(\nabla\xi_0 \otimes \nabla\xi_0)] = 0 & \text{in } \ \Omega_R, \\ [\mathbb{C}\nabla \boldsymbol{u}_0 + \dfrac{\varepsilon}{2}\mathbb{T}(\nabla\xi_0 \otimes \nabla\xi_0)]\boldsymbol{n} = 0 & \text{on } \ \partial\Omega_R, \\ \operatorname{div}(-\varepsilon\nabla\xi_0) = \rho_e & \text{in } \ \Omega_R, \\ \xi_0 = 0 & \text{on } \ \{x = -L_2 \text{ or } L_1\}, \end{cases} \tag{D.7}$$

where ρ_e represents a surface charge layer as shown in Figure 10. Upon applying a potential difference such that $V_1 - V_2 = V$, again by (D.6) the final state satisfies

$$\begin{cases} \operatorname{div}[\mathbb{C}\nabla \boldsymbol{u}_f - \hat{\beta}(T_f - T_0)\boldsymbol{I} + \dfrac{\varepsilon}{2}\mathbb{T}(\nabla\xi_f \otimes \nabla\xi_f)] = 0 & \text{in } \ \Omega_R, \\ [\mathbb{C}\nabla \boldsymbol{u}_f - \hat{\beta}(T_f - T_0)\boldsymbol{I} + \dfrac{\varepsilon}{2}\mathbb{T}(\nabla\xi_f \otimes \nabla\xi_f)]\boldsymbol{n} = 0 & \text{on } \ \partial\Omega_R, \\ \operatorname{div}(-\varepsilon\nabla\xi_f) = \rho_e & \text{in } \ \Omega_R. \\ \xi_f = V_1 \text{ (resp. } V_2) \text{ on } \ \{x = L_1\}(\text{resp. } \{x = -L_2\}). \end{cases} \tag{D.8}$$

To use first law of thermodynamic according to Eq.(2.66),we compute the total work done to the system by Eq.(2.15)

$$W^e = \int P_{\text{ext}} dt = \int_{\Omega_R} \varepsilon\nabla\xi_f \cdot \nabla(\xi_f - \xi_0). \tag{D.9}$$

and the internal energy density Φ may be written as

$$\Phi(\boldsymbol{F}, \boldsymbol{P}, T) = \Psi_0 + CT + \hat{\beta}T_0 \operatorname{Tr}\boldsymbol{H} + \frac{1}{2}\boldsymbol{H} \cdot \mathbb{C}\boldsymbol{H} + \frac{1}{2}\boldsymbol{P} \cdot \boldsymbol{\chi}\boldsymbol{P} + \boldsymbol{H} \cdot \mathbb{M}(\boldsymbol{P} \otimes \boldsymbol{P})$$

Therefore, by Eq.(2.5) we find that

$$\begin{aligned} U_f - U_0 = \int_{\Omega_R} \Big[& C(T_f - T_0) + \hat{\beta}T_0\nabla \cdot (\boldsymbol{u}_f - \boldsymbol{u}_0) + \frac{\varepsilon}{2}(|\nabla\xi_f|^2 - |\nabla\xi_0|^2) \\ & + \frac{1}{2}(\nabla \boldsymbol{u}_f) \cdot \mathbb{C}(\nabla \boldsymbol{u}_f) - \frac{1}{2}(\nabla \boldsymbol{u}_0) \cdot \mathbb{C}(\nabla \boldsymbol{u}_0) \\ & - \frac{1}{2}(\varepsilon - \varepsilon_0)|\nabla\xi_f|^2\nabla \cdot \boldsymbol{u}_f + \frac{1}{2}(\varepsilon - \varepsilon_0)|\nabla\xi_0|^2\nabla \cdot \boldsymbol{u}_0 \Big]. \end{aligned} \tag{D.10}$$

Inserting (D.9) and (D.10) into Eq.(2.66) and neglecting $O(\eta^2)$-terms according to the scaling assumption (D.1), we find that

$$\begin{aligned} 0 = U_f - U_0 - W^e \approx \int_{\Omega_R} \Big[& C(T_f - T_0) + \hat{\beta}T_0\nabla \cdot (\boldsymbol{u}_f - \boldsymbol{u}_0) \\ & - \frac{\varepsilon}{2}(|\nabla(\xi_f - \xi_0)|^2) \Big]. \end{aligned} \tag{D.11}$$

Solving (D.11) together with (D.7) and (D.8) for 1-D reduces to

$$\begin{cases} (\lambda_1 - 1) - \dfrac{\varepsilon_1 \varepsilon_2 V}{2E_1} \dfrac{(2qL_2 - \varepsilon_2 V)}{(\varepsilon_1 L_2 + \varepsilon_2 L_1)^2} - \alpha_1 (T_f - T_0) = 0, \\ (\lambda_2 - 1) + \dfrac{\varepsilon_1 \varepsilon_2 V}{2E_2} \dfrac{(2qL_1 + \varepsilon_1 V)}{(\varepsilon_1 L_2 + \varepsilon_2 L_1)^2} - \alpha_2 (T_f - T_0) = 0. \\ (C_1 L_1 + C_2 L_2)(T_f - T_0) + \alpha_1 E_1 L_1 T_0 (\lambda_1 - 1) + \alpha_2 E_2 L_2 T_0 (\lambda_2 - 1) \\ - \dfrac{\varepsilon_1}{2} L_1 (\dfrac{V_1}{L_1})^2 - \dfrac{\varepsilon_2}{2} L_2 (\dfrac{V_2}{L_2})^2 = 0 \end{cases} \tag{D.12}$$

Where E stands for the material's elastic modulus. Neglecting the effect of electric field on the thickness (as it is comparably small for linear regions) we obtain:

$$T_f - T_0 = \frac{\dfrac{\varepsilon_1}{2L_1} V_1^2 + \dfrac{\varepsilon_2}{2L_2} V_2^2}{C_1 L_1 + C_2 L_2 + (\alpha_1^2 E_1 L_1 + \alpha_2^2 E_2 L_2) T_0} \tag{D.13}$$

References

[AC93] Michael F Ashby and D Cebon. Materials selection in mechanical design. *Le Journal de Physique IV*, 3(C7):C7–1, 1993.

[ADLS15] Zeinab Alameh, Qian Deng, Liping Liu, and Pradeep Sharma. Using electrets to design concurrent magnetoelectricity and piezoelectricity in soft materials. *Journal of Materials Research*, 30(1):93–100, 2015.

[Ahm12] Zulkifli Ahmad. Polymeric dielectric materials. *Dielectric Material*, pages 3–26, 2012.

[AUV06] Sheikh N Ahmad, CS Upadhyay, and C Venkatesan. Electro-thermo-elastic formulation for the analysis of smart structures. *Smart materials and structures*, 15(2):401, 2006.

[BBGG+14] Siegfried Bauer, Simona Bauer-Gogonea, Ingrid Graz, Martin Kaltenbrunner, Christoph Keplinger, and Reinhard Schwödiauer. 25th anniversary article: a soft future: from robots and sensor skin to energy harvesters. *Advanced Materials*, 26(1):149–162, 2014.

[BGMS04] Siegfried Bauer, Reimund Gerhard-Multhaupt, and Gerhard M Sessler. Ferroelectrets: Soft electroactive foams for transducers. 2004.

[BIG+89] Johannes Brandrup, Edmund Heinz Immergut, Eric A Grulke, Akihiro Abe, and Daniel R Bloch. *Polymer handbook*, volume 7. Wiley New York etc, 1989.

[BP89] Siegfried Bauer and Bernd Ploss. A simple technique to interface pyroelectric materials with silicon substrates for infrared detection. *Ferroelectrics Letters Section*, 9(6):155–160, 1989.

[Bro63] William Fuller Brown. *Micromagnetics*. Number 18. Interscience Publishers, 1963.

[BSB08] Gerda Buchberger, Reinhard Schwödiauer, and Siegfried Bauer. Flexible large area ferroelectret sensors for location sensitive touchpads. *Applied Physics Letters*, 92(12):123511, 2008.

[BTL+14] CR Bowen, J Taylor, E LeBoulbar, D Zabek, A Chauhan, and R Vaish. Pyroelectric materials and devices for energy harvesting applications. *Energy & Environmental Science*, 7(12):3836–3856, 2014.

[CBDR10] Federico Carpi, Siegfried Bauer, and Danilo De Rossi. Stretching dielectric elastomer performance. *Science*, 330(6012):1759–1761, 2010.

[CEG78] KL Chowdhury, Marcelo Epstein, and PG Glockner. On the thermodynamics of non-linear elastic dielectrics. *International Journal of Non-Linear Mechanics*, 13(5):311–322, 1978.

[CG77] KL Chowdhury and Peter G Glockner. On thermoelastic dielectrics. *International journal of solids and structures*, 13(11):1173–1182, 1977.

[DB07] Kaushik Dayal and Kaushik Bhattacharya. A real-space non-local phase-field model of ferroelectric domain patterns in complex geometries. *Acta materialia*, 55(6):1907–1917, 2007.

[DLS14] Qian Deng, Liping Liu, and Pradeep Sharma. Electrets in soft materials: Nonlinearity, size effects, and giant electromechanical coupling. *Physical Review E*, 90(1):012603, 2014.

[GFA10] Morton E Gurtin, Eliot Fried, and Lallit Anand. *The mechanics and thermodynamics of continua*. Cambridge University Press, 2010.

[GM87] R Gerhard-Multhaupt. Electrets: Dielectrics with quasi-permanent charge or polarization. *IEEE transactions on electrical insulation*, (5):531–554, 1987.

[GS98] DH Gracias and GA Somorjai. Continuum force microscopy study of the elastic modulus, hardness and friction of polyethylene and polypropylene surfaces. *Macromolecules*, 31(4):1269–1276, 1998.

[HS08] J Hillenbrand and GM Sessler. Dc-biased ferroelectrets with large piezoelectric d 33-coefficients. *Journal of applied physics*, 103(7):074103, 2008.

[HSSC13] Jiangshui Huang, Samuel Shian, Zhigang Suo, and David R Clarke. Maximizing the energy density of dielectric elastomer generators using equi-biaxial loading. *Advanced Functional Materials*, 23(40):5056–5061, 2013.

[JA18] R Jayendiran and A Arockiarajan. Theoretical modeling and experimental characterization of rate and temperature dependent electromechanical behavior of piezocomposites. *European Journal of Mechanics-A/Solids*, 69:23–44, 2018.

[Jam02] RD James. Configurational forces in magnetism with application to the dynamics of a small-scale ferromagnetic shape memory cantilever. *Continuum Mechanics and Thermodynamics*, 14(1):55–86, 2002.

[KFRP08] Do Hoon Kim, Paula D Fasulo, William R Rodgers, and DR Paul. Effect of the ratio of maleated polypropylene to organoclay on the structure and properties of tpo-based nanocomposites. part ii: Thermal expansion behavior. *Polymer*, 49(10):2492–2506, 2008.

[KGBA16] Taylor Kelly, Bahar Moradi Ghadi, Sean Berg, and Haleh Ardebili. In situ study of strain-dependent ion conductivity of stretchable polyethylene oxide electrolyte. *Scientific reports*, 6:20128, 2016.

[LCM05] Stephen B Long, Ernest B Campbell, and Roderick MacKinnon. Voltage sensor of kv1. 2: structural basis of electromechanical coupling. *Science*, 309(5736):903–908, 2005.

[Liu13] Liping Liu. On energy formulations of electrostatics for continuum media. *Journal of the Mechanics and Physics of Solids*, 61(4):968–990, 2013.

[Liu14] Liping Liu. An energy formulation of continuum magneto-electro-elasticity with applications. *Journal of the Mechanics and Physics of Solids*, 63:451–480, 2014.

[LLP17] Victor Lefevre and Oscar Lopez-Pamies. Homogenization of elastic dielectric composites with rapidly oscillating passive and active source terms. *SIAM Journal on Applied Mathematics*, 77(6):1962–1988, 2017.

[LS18] Liping Liu and Pradeep Sharma. Emergent electromechanical coupling of electrets and some exact relations—the effective properties of soft materials with embedded external charges and dipoles. *Journal of the Mechanics and Physics of Solids*, 112:1–24, 2018.

[MHS16] Markus Mehnert, Mokarram Hossain, and Paul Steinmann. On nonlinear thermo-electro-elasticity. *Proc. R. Soc. A*, 472(2190):20160170, 2016.

[MKR+08] Bernhard Joachim Mokross, M Kollosche, T Ruscher, G Kofod, and R Gerhard. Thermodynamic modeling of pyroelectric and piezoelectric properties of cellular polymers. *Physical Review B*, 78(23):235407, 2008.

[MPS17] Markus Mehnert, Jean-Paul Pelteret, and Paul Steinmann. Numerical modelling of nonlinear thermo-electro-elasticity. *Mathematics and Mechanics of Solids*, 22(11):2196–2213, 2017.

[MXLM11] Poorna Mane, Jingsi Xie, Kam K Leang, and Karla Mossi. Cyclic energy harvesting from pyroelectric materials. *IEEE transactions on ultrasonics, ferroelectrics, and frequency control*, 58(1):10–17, 2011.

[Nal95] Hari Singh Nalwa. *Ferroelectric polymers: chemistry: physics, and applications*. CRC Press, 1995.

[NSBG+01] Gerhard S Neugschwandtner, Reinhard Schwödiauer, Simona Bauer-Gogonea, Siegfried Bauer, Mika Paajanen, and Jukka Lekkala. Piezo-and pyroelectricity of a polymer-foam space-charge electret. *Journal of Applied Physics*, 89(8):4503–4511, 2001.

[PJK59] FJ Padden Jr and HD Keith. Spherulitic crystallization in polypropylene. *Journal of Applied Physics*, 30(10):1479–1484, 1959.

[Qiu10] Xunlin Qiu. Patterned piezo-, pyro-, and ferroelectricity of poled polymer electrets. *Journal of Applied physics*, 108(1):8, 2010.

[RSH10] John A Rogers, Takao Someya, and Yonggang Huang. Materials and mechanics for stretchable electronics. *Science*, 327(5973):1603–1607, 2010.

[SCB10] Martin Stråat, Igor Chmutin, and Antal Boldizar. Dielectric properties of polyethylene foams at medium and high frequencies. In *Transactons of the Nordic Rheology Society*, volume 18, pages 107–116, 2010.

[Sch88] G Schwarz. Thermal expansion of polymers from 4.2 k to room temperature. *Cryogenics*, 28(4):248–254, 1988.

[SH99] GM Sessler and J Hillenbrand. Electromechanical response of cellular electret films. In *Electrets, 1999. ISE 10. Proceedings. 10th International Symposium on*, pages 261–264. IEEE, 1999.

[SOS+91] Yukio Sakashita, Toshiyuki Ono, Hideo Segawa, Kouji Tominaga, and Masaru Okada. Preparation and electrical properties of mocvd-deposited pzt thin films. *Journal of Applied Physics*, 69(12):8352–8357, 1991.

[SS80] Gerhard M Sessler and Keshawa Shahi. Electrets, topics in applied physics. *Journal of The Electrochemical Society*, 127(12):530C–530C, 1980.

[SVS14] Prashant Saxena, Duc Khoi Vu, and Paul Steinmann. On rate-dependent dissipation effects in electro-elasticity. *International Journal of Non-Linear Mechanics*, 62:1–11, 2014.

[Val12] Matjaz Valant. Electrocaloric materials for future solid-state refrigeration technologies. *Progress in Materials Science*, 57(6):980–1009, 2012.

[VBPCB13] Rocco Vertechy, Giovanni Berselli, Vincenzo Parenti Castelli, and Massimo Bergamasco. Continuum thermo-electro-mechanical model for electrostrictive elastomers. *Journal of Intelligent Material Systems and Structures*, 24(6):761–778, 2013.

[Vol16] Konstantin Volokh. *Mechanics of soft materials*. Springer, 2016.

[VTSWdH99] J Van Turnhout, RE Staal, M Wubbenhorst, and PH de Haan. Distribution and stability of charges in porous polypropylene films. In *Electrets, 1999. ISE 10. Proceedings. 10th International Symposium on*, pages 785–788. IEEE, 1999.

[VYP08] Damien Vanderpool, Jeong Hwan Yoon, and Laurent Pilon. Simulations of a prototypical device using pyroelectric materials for harvesting waste heat. *International Journal of Heat and Mass Transfer*, 51(21):5052–5062, 2008.

[WB05] Michael Wegener and Siegfried Bauer. Microstorms in cellular polymers: A route to soft piezoelectric transducer materials with engineered macroscopic dipoles. *ChemPhysChem*, 6(6):1014–1025, 2005.

[WE14] John G Webster and Halit Eren. *Measurement, instrumentation, and sensors handbook: electromagnetic, optical, radiation, chemical, and biomedical measurement*. CRC press, 2014.

[Wha86] RW Whatmore. Pyroelectric devices and materials. *Reports on progress in physics*, 49(12):1335, 1986.

[WSJ76] R Watton, C Smith, and GR Jones. Pyroelectric materials: Operation and performance in the pyroelectric camera tube. *Ferroelectrics*, 14(1):719–721, 1976.

[XB08] Yu Xiao and Kaushik Bhattacharya. A continuum theory of deformable, semiconducting ferroelectrics. *Archive for Rational Mechanics and Analysis*, 189(1):59–95, 2008.

[XMG+10] J Xie, XP Mane, CW Green, KM Mossi, and Kam K Leang. Performance of thin piezoelectric materials for pyroelectric energy harvesting. *Journal of Intelligent Material Systems and Structures*, 21(3):243–249, 2010.

[YD11] Lun Yang and Kaushik Dayal. A completely iterative method for the infinite domain electrostatic problem with nonlinear dielectric media. *Journal of Computational Physics*, 230(21):7821–7829, 2011.

[YZS17] Shengyou Yang, Xuanhe Zhao, and Pradeep Sharma. Avoiding the pull-in instability of a dielectric elastomer film and the potential for increased actuation and energy harvesting. *Soft Matter*, 2017.

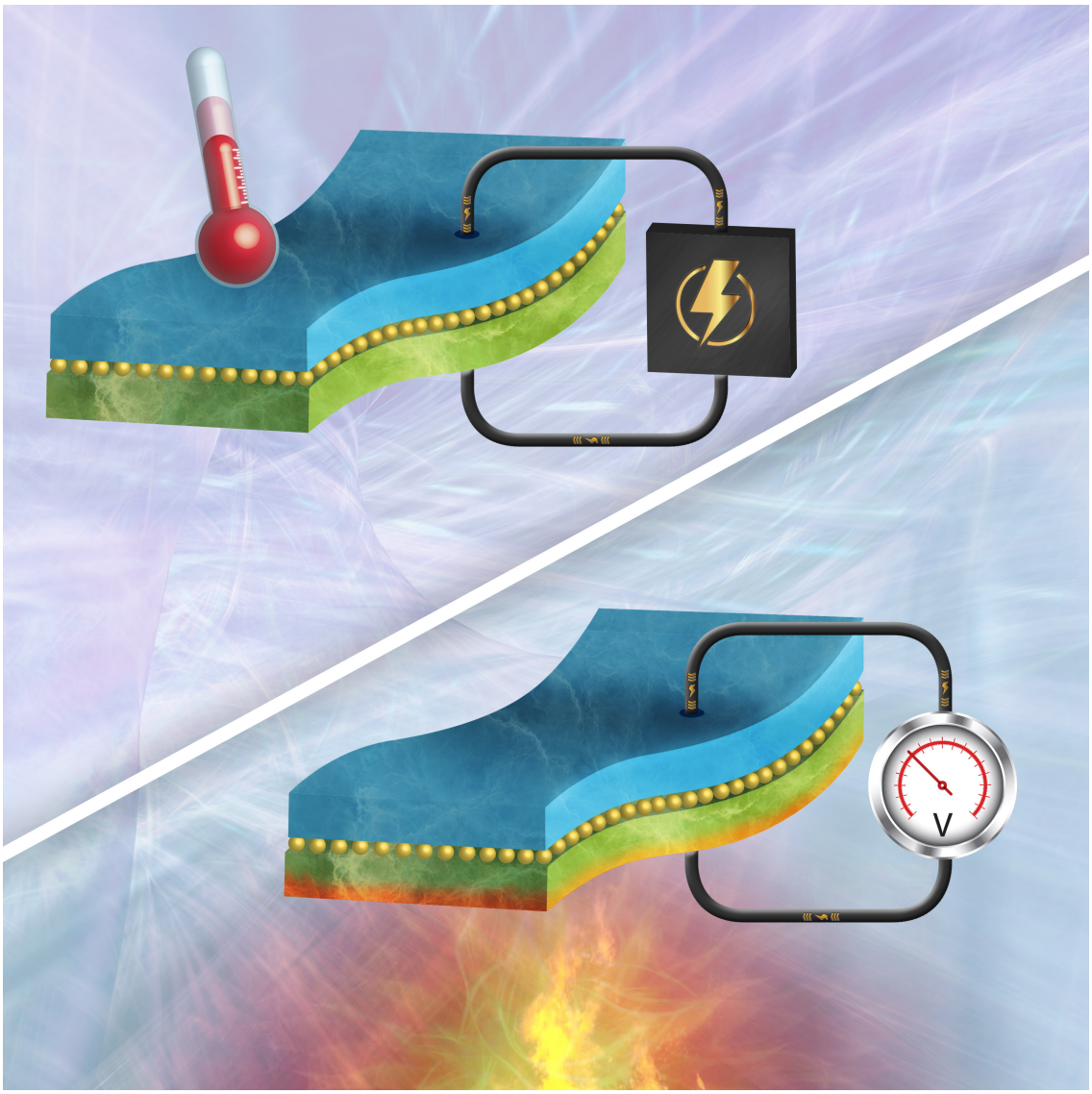

Figure 2 A schematic showing the use of electrets to create apparent pyroelectric and/or electrocaloric behavior from otherwise non-pyroelectric soft materials by embedding charges in layered thin films. In principle, alternative configurations such as polymer foams may be also possible.

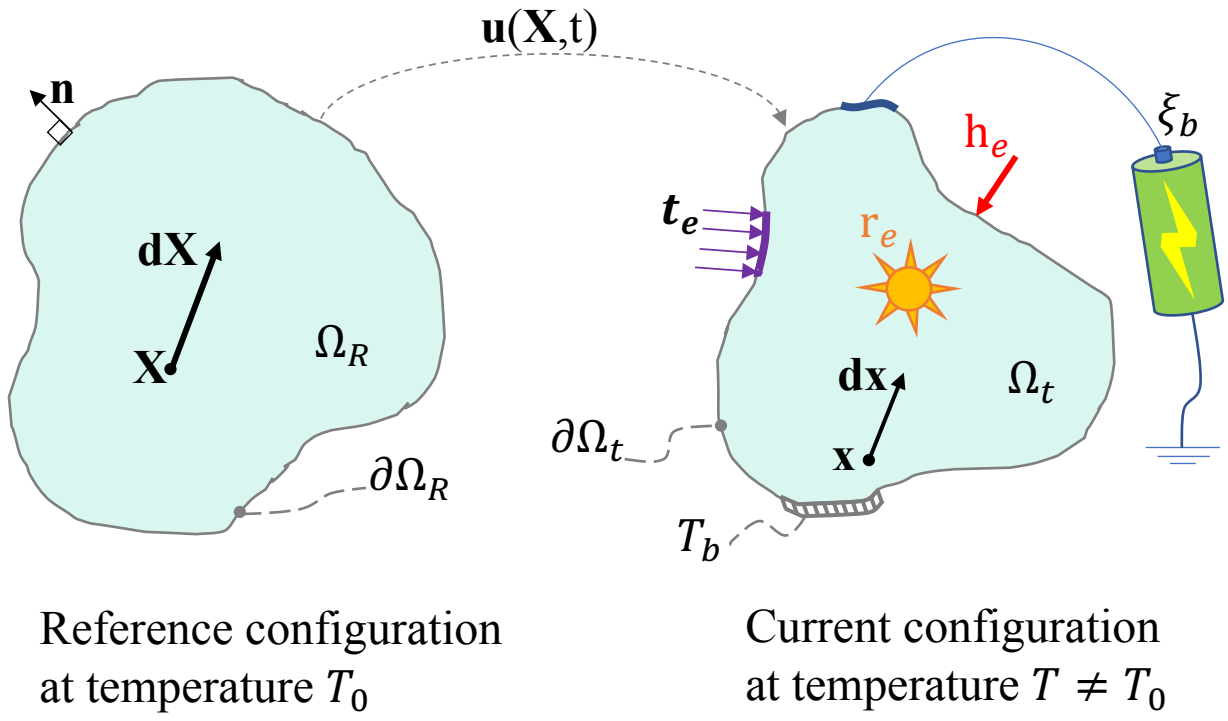

Figure 3 Thermo-electro-mechanical system: Ω_R and Ω_t are the reference and spatial configurations of the system, and $\partial\Omega_R$ and $\partial\Omega_t$ are the according boundaries. $\boldsymbol{X}$ and $\boldsymbol{x}$ represent the position of the material in Lagrangian and Eulerian coordinates and $\mathbf{n}$ is the unit outward vector. $\mathbf{t_e}$ and h_e are the traction and heat flux applied to the system. T_0 is the initial temperature of the system and T_b corresponds to the temperature boundary condition. r_e is the heat source, ξ_b is the electrical potential, and $\boldsymbol{u}$ is the displacement vector.

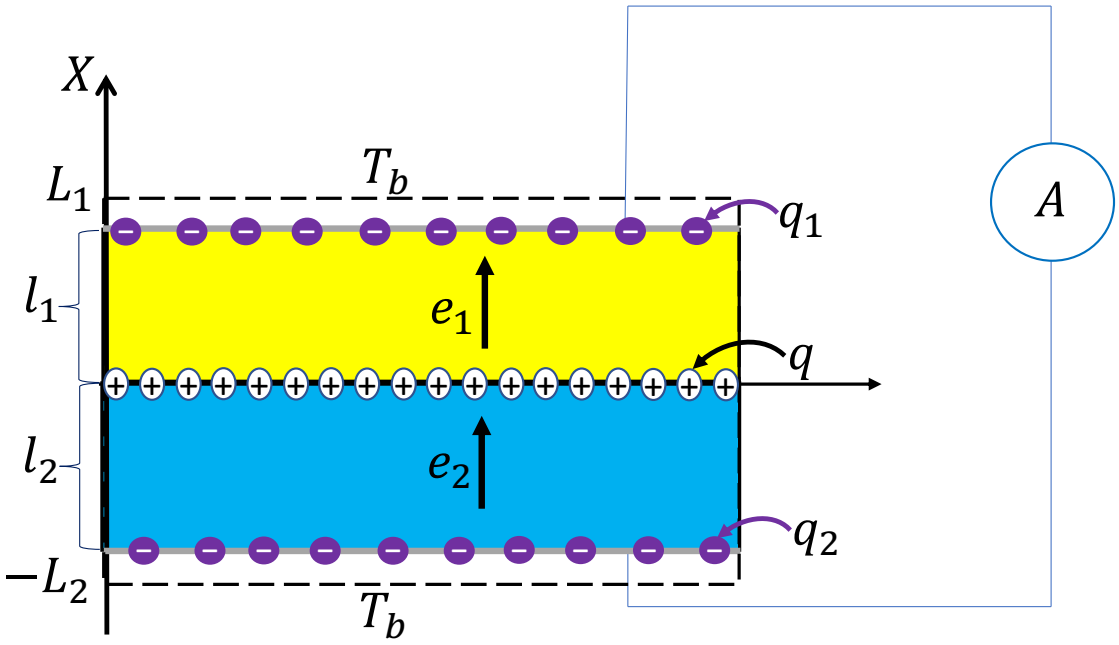

Figure 4 Temperature difference applied to the two-film layered electret consisting of embedded charge q at the interface (Figure 1), and induced charges q_1 and q_2 at the upper and lower surfaces. Dashed lines shows the undeformed structure. L_1 and L_2 represent the reference thicknesses of layers and l_1 and l_2 are the thicknesses for the deformed structure.

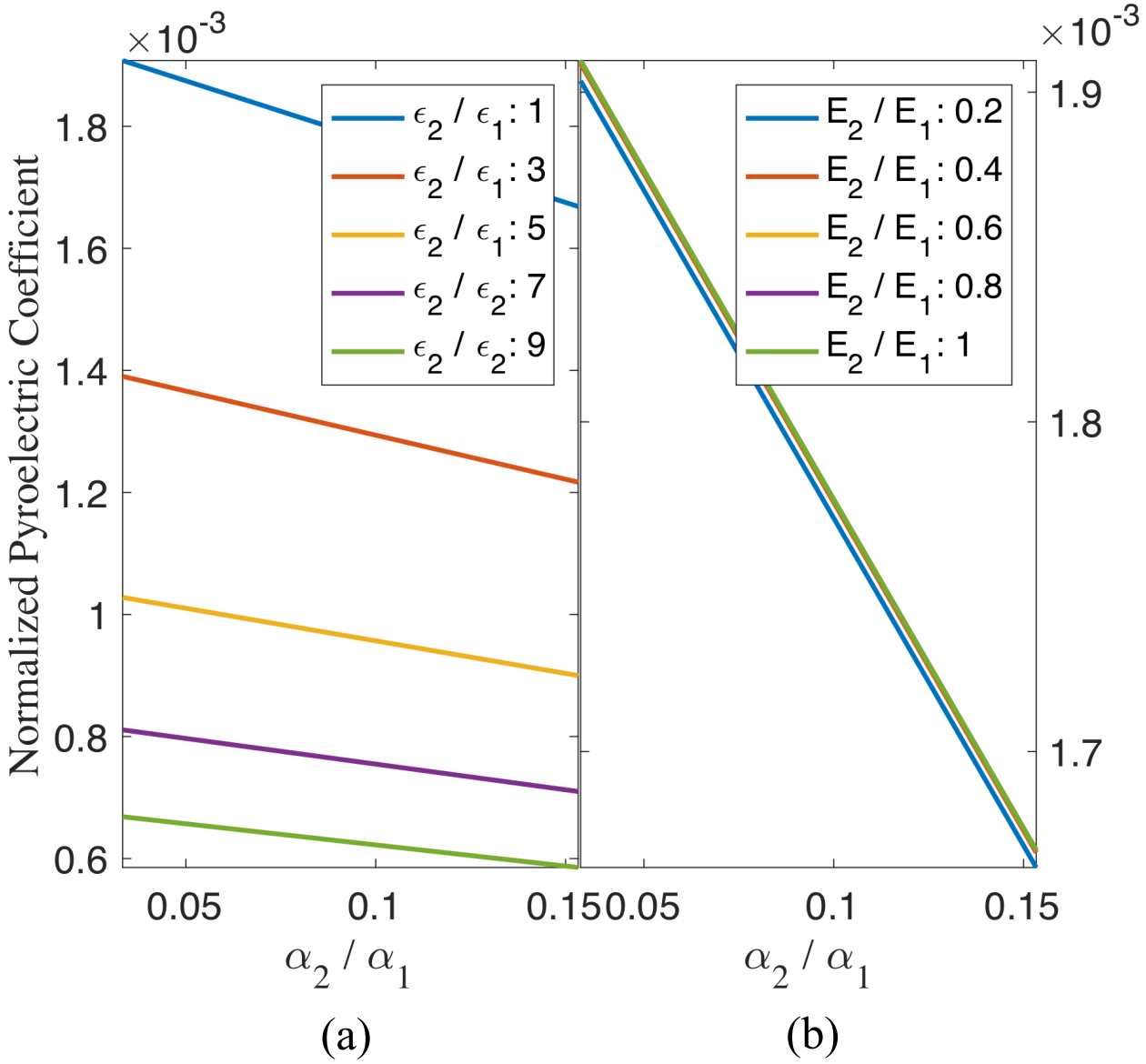

Figure 5 Eq.(2.56):
Variation of normalized pyroelectric coefficient with respect to the value of the best well known pyroelectric material – the PZT oriented thin film ($3 \times 10^{-4} C/m^2 K$) [SOS+91]. The pyroelectric coefficient is plotted with respect to the ratio of thermal expansion coefficient for the electret schematically shown in Figure 4. The left panel shows the effect of dielectric constant when the second layer's elastic modulus is set to be $0.7MPa$ and the right panel shows the effect of elastic modulus when the dielectric ratio of the layers is one. In both cases the first layer's properties are the same as in Table 1. Both layers have the same thickness ($70\mu m$), and the electric charge density at the interface and the temperature difference are $0.002C/m^2$ and $10°C$, respectively.

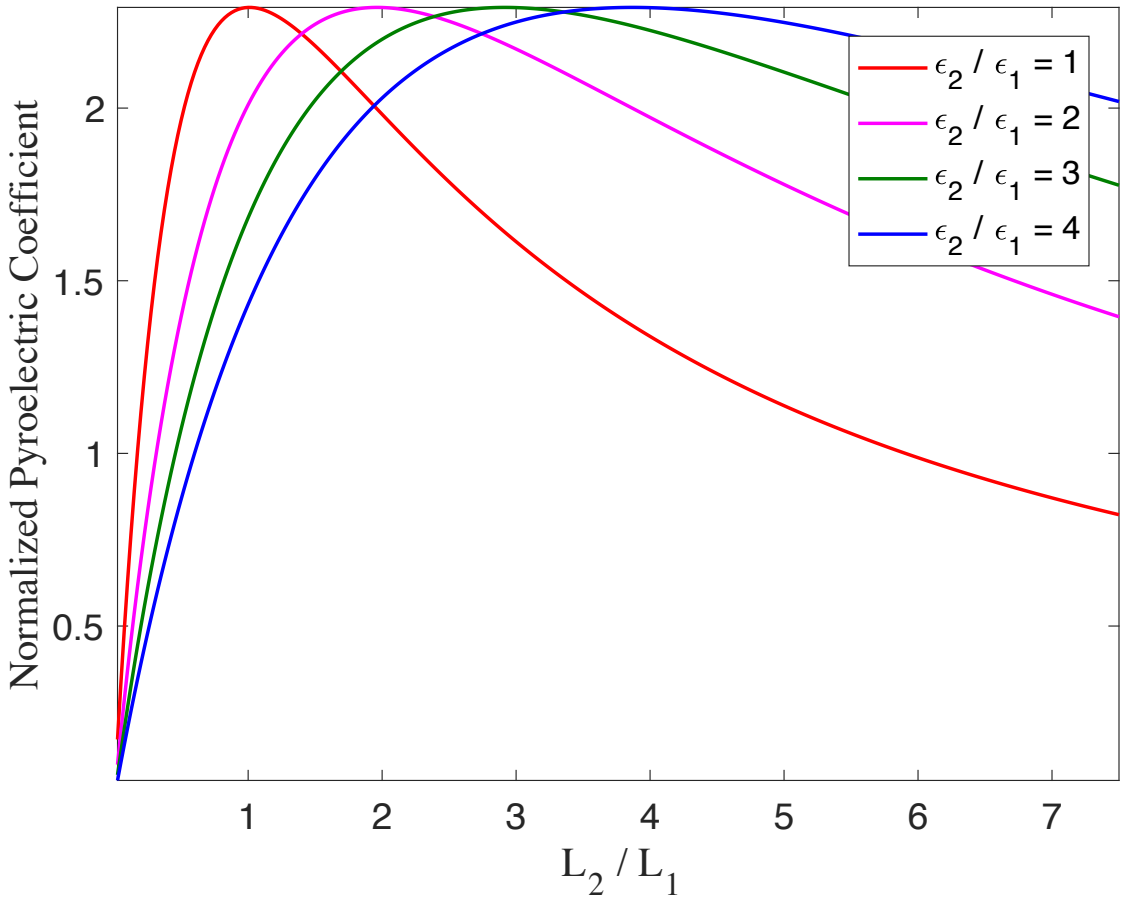

Figure 6 Variation of pyroelectric coefficient normalized with respect to the experimental value of Bauer and co-workers [NSBG+01] ($2.5 \times 10^{-7} C/m^2 K$) [SOS+91] for the electret shown in Figure 4. In that, $\varepsilon_1 = \varepsilon_0$, $\alpha_1 = 1.2 \times 10^{-3} K^{-1}$, $\alpha_2 = 4 \times 10^{-5} K^{-1}$, $L_1 = 70 \mu m$, $q = 0.002 C/m^2$, $\Delta T = 10^{\circ} C$, and both layers' elastic modulus is $1 MPa$.

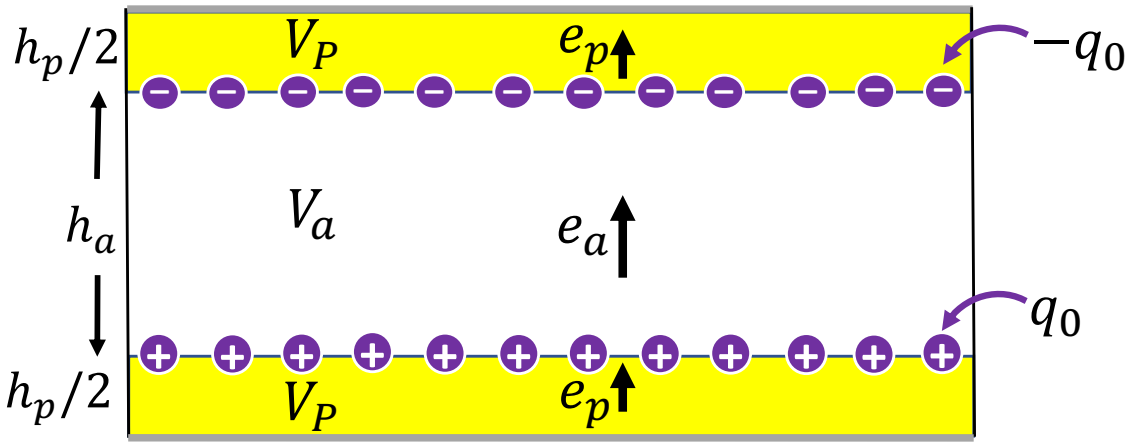

Figure 7 A simplified model for the porous cellular polymer electret with opposite charges on the surfaces of voids.

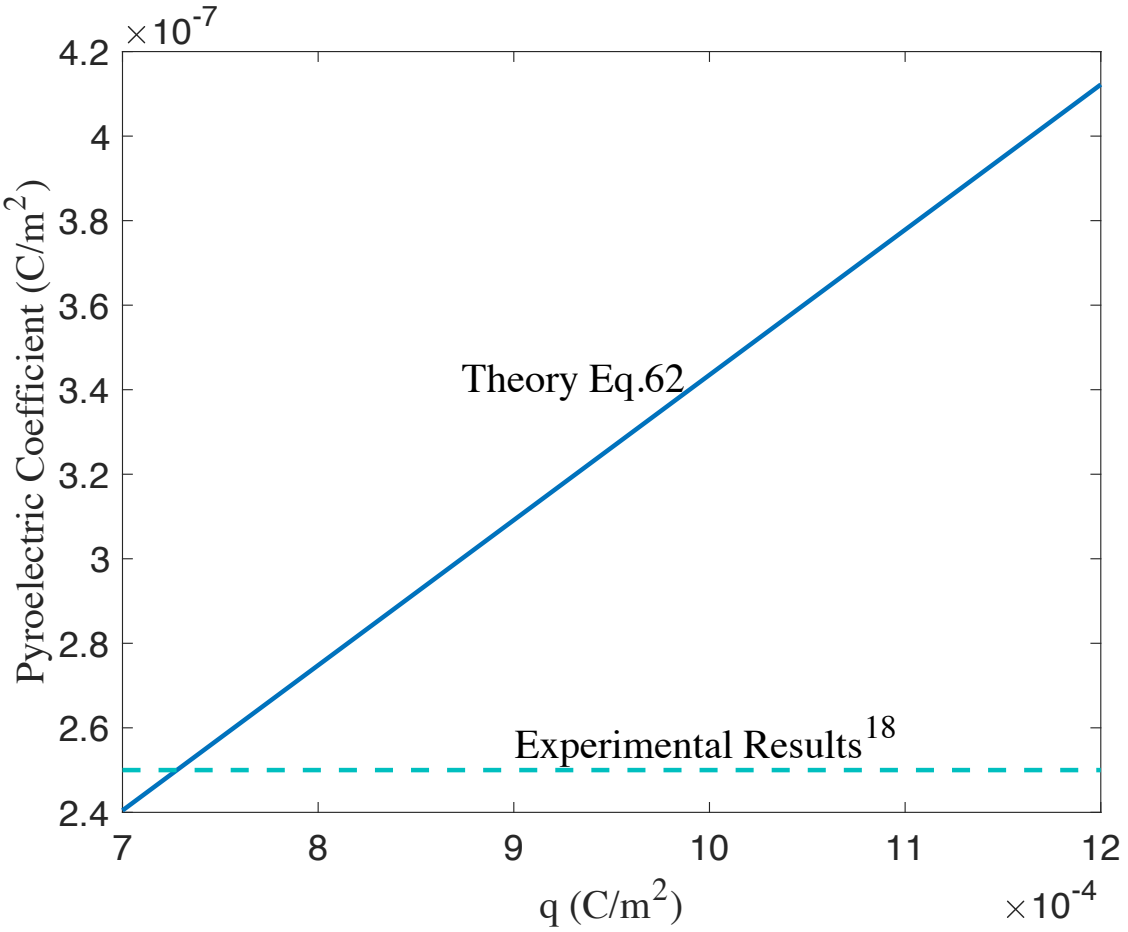

Figure 8 Variation of pyroelectric coefficient for the porous electret shown in Figure 7 with respect to the charge density at the interface. Here, $\varepsilon_p = 2.2\varepsilon_0$, $H_p = 26\mu m$, $H_a = 44\mu m$, $T = 25°C$, and $\Delta T = 10°C$.

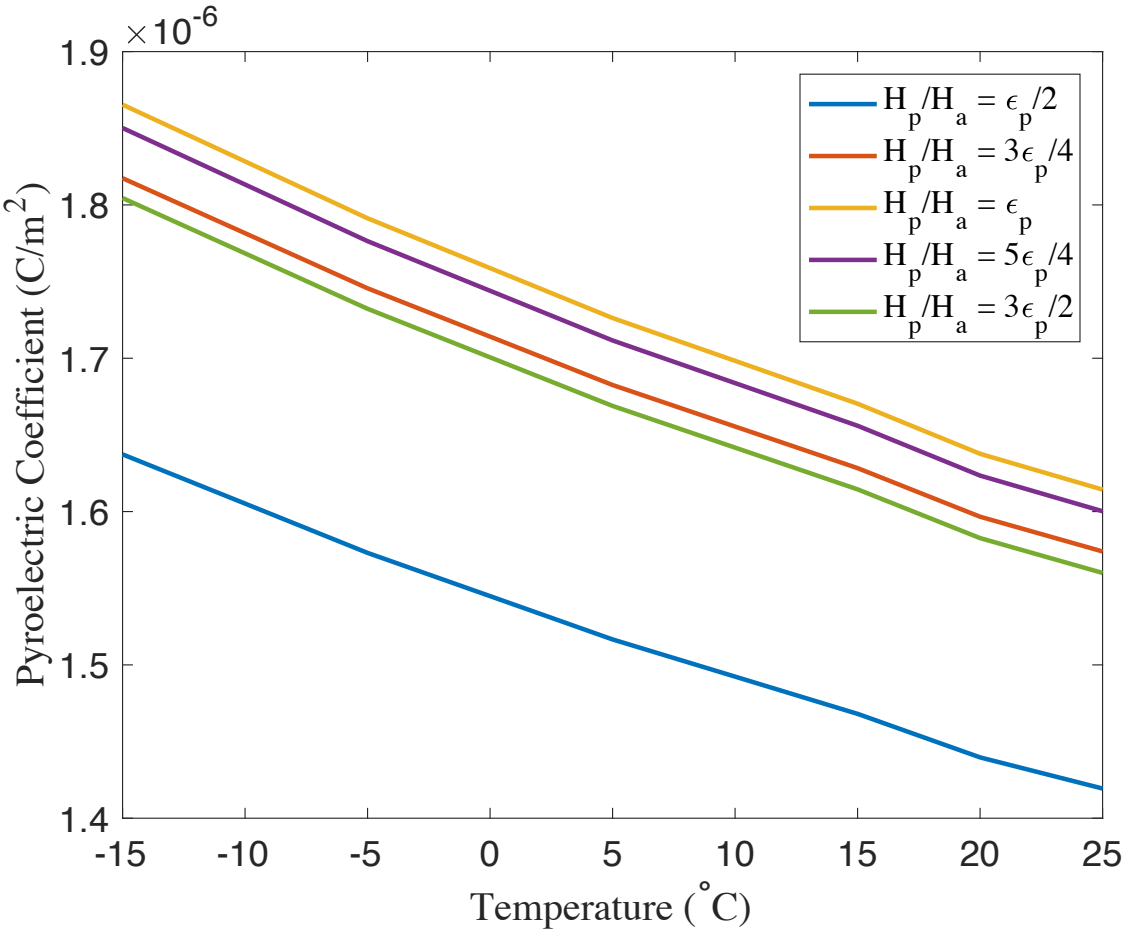

Figure 9 Variation of pyroelectric coefficient with respect to temperature for the porous electret shown in Figure 7. The polymer is polyimide with $\varepsilon_p = 2.8\varepsilon_0$ [Ahm12], $\alpha_p = 4 \times 10^{-5}/K$ [Sch88], $q = 0.002C/m^2$, $\Delta T = 10°C$.

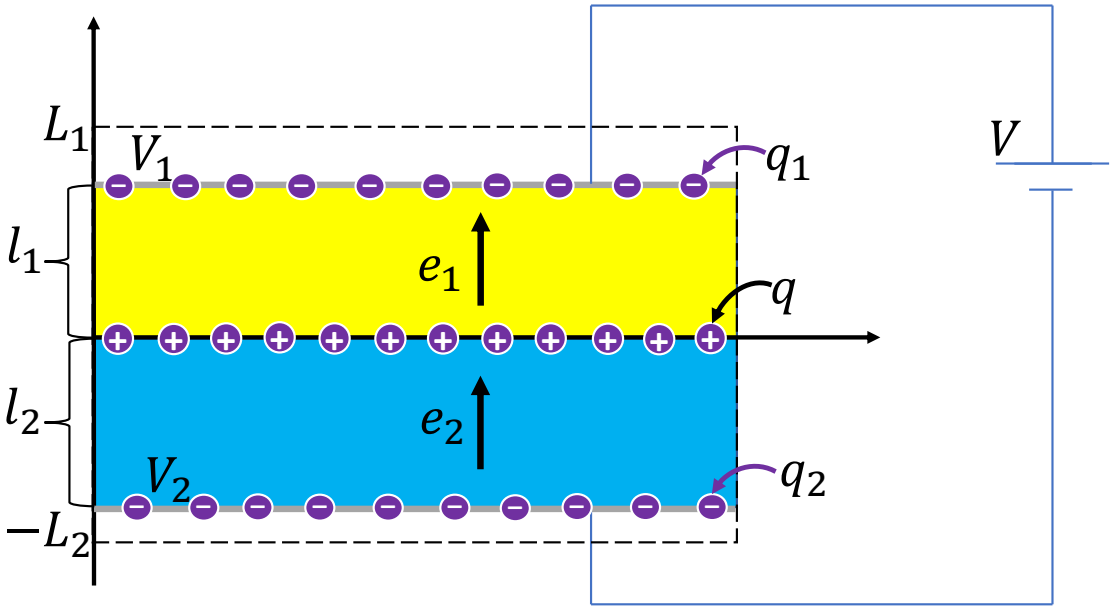

Figure 10 Voltage difference applied to bilayer film structure with embedded charge q at the interface (Figure 1), and induced charges q_1 and q_2 at the upper and lower surfaces. Adiabatic boundary conditions are assumed. the dashed line shows the undeformed structure. L_1 and L_2 represent the reference thickness of each layer and l_1 and l_2 are the thicknesses of the deformed structure.

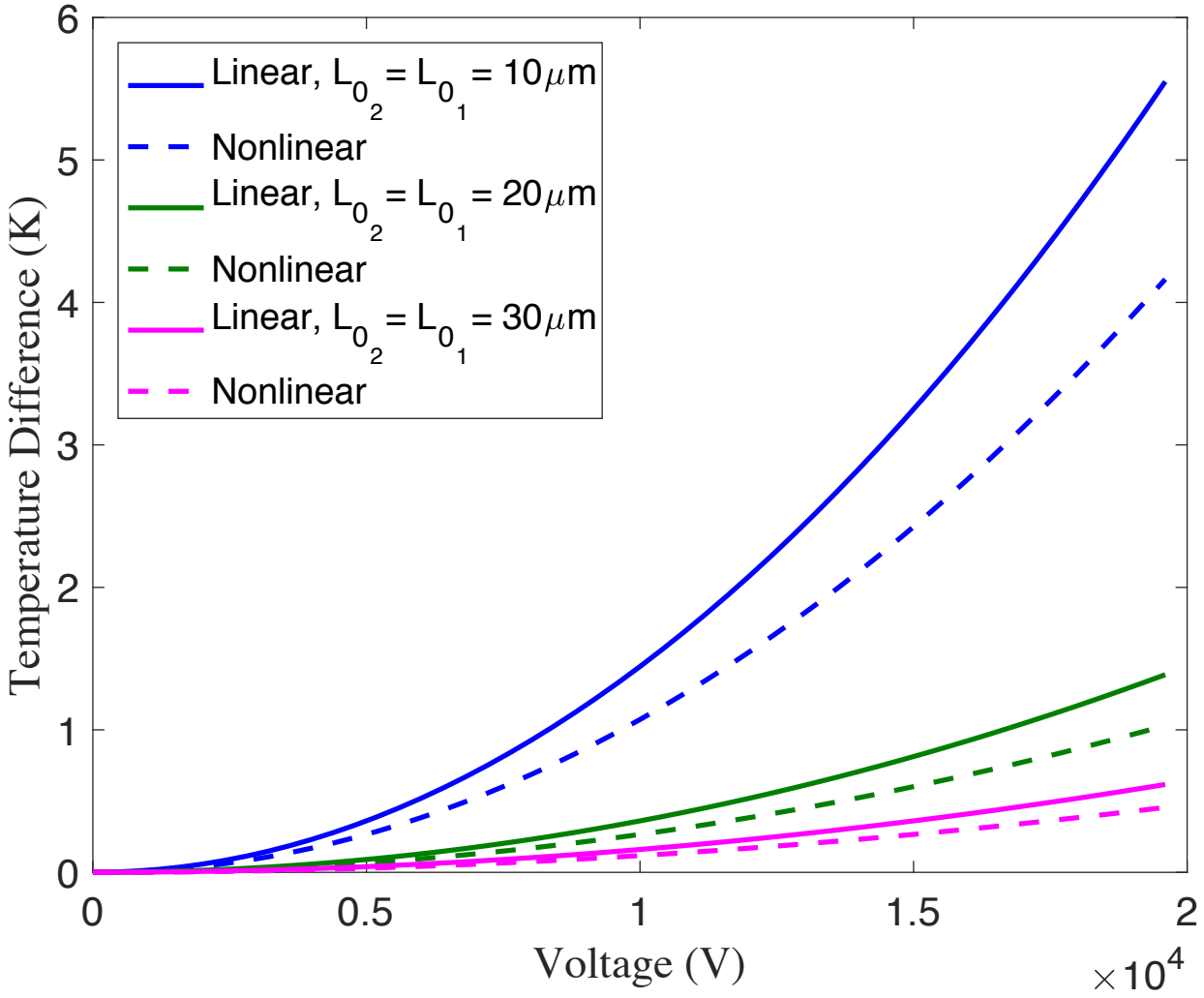

Figure 11 Temperature difference with respect to the voltage applied to the system schematically shown in Figure 10. The materials are polypropylene and polyethylene at room temperature with material properties recorded in Table 2 and the electric charge density at the interface is $0.002C/m^2$.

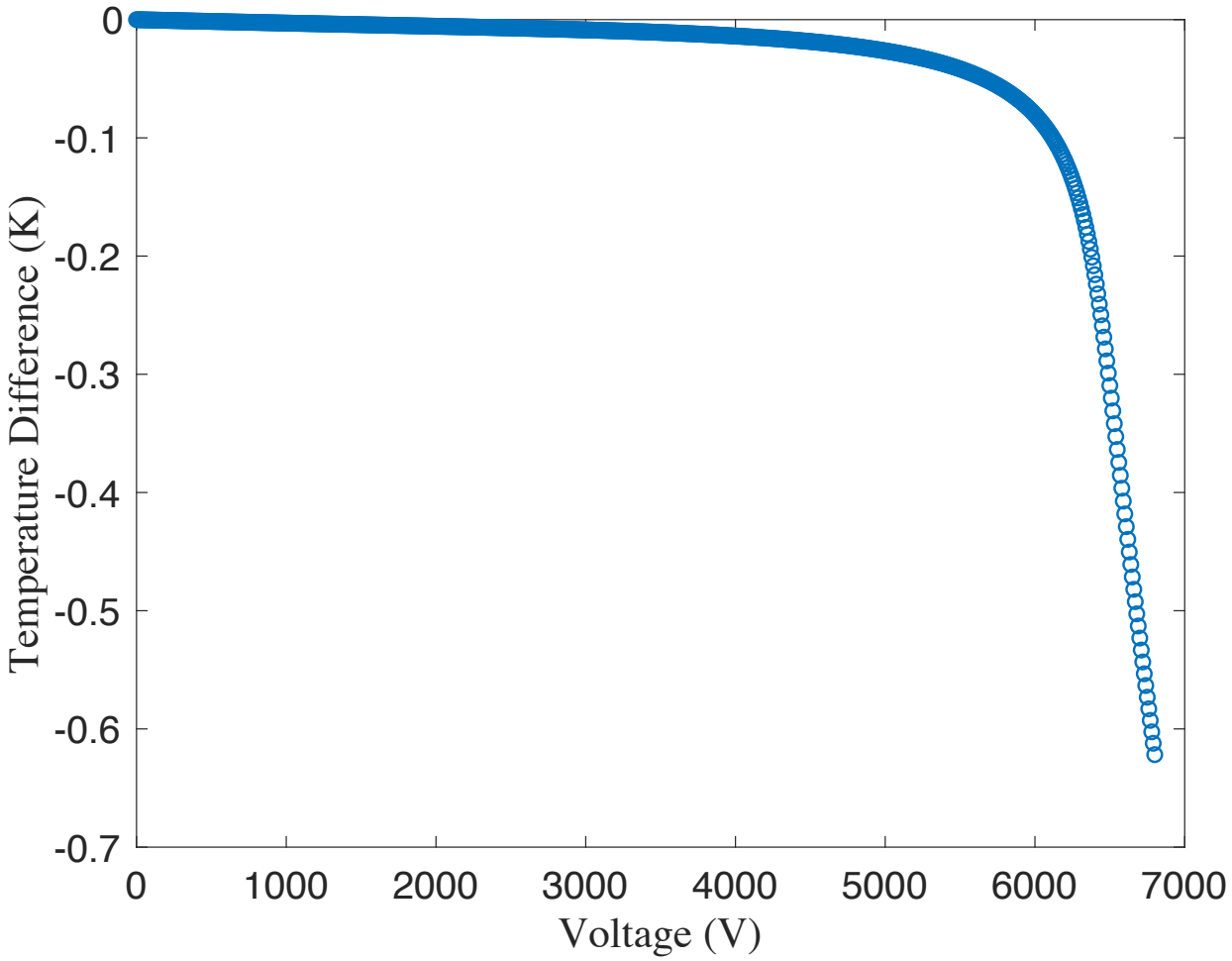

Figure 12 Temperature difference with respect to the voltage applied to the system schematically shown in Figure 7. The electret is initially at room temperature, polymer is polypropylene with $C_p = 1920 J/KgK$, $\rho_p = 904 Kg/m^3$, $\alpha_p = 8 \times 10^{-5} K^{-1}$, $\mu_p = 400 MPa$, $E = 0.8 MPa$, $\varepsilon_p = 2.35\varepsilon_0$, $H_p = 32\mu m$, $H_a = 38\mu m$, $\alpha_a = 3.4 \times 10^{-3} K^{-1}$, $C_a = 1000 J/KgK$, $\rho_a = 1.2 Kg/m^3$ and the electric charge density at the interface is $0.001 C/m^2$.